Published in final edited form as:
J Proteome Res. 2014 February 7; 13(2): 1112–1127. doi:10.1021/pr4012359.

Systematic Nucleo-Cytoplasmic Trafficking of Proteins Following Exposure of MCF7 Breast Cancer Cells to Estradiol

Gabriella Pinto[†,‡], **Abdulrab Ahmed M. Alhaiek**[†], **Sepan Amadi**[†], **Amal T. Qattan**[†], **Mark Crawford**[†], **Marko Radulovic**[†], and **Jasminka Godovac-Zimmermann**[*,†]

[†]Proteomics and Molecular Cell Dynamics, Center for Nephrology, Division of Medicine, School of Life and Medical Sciences, University College London, Royal Free Campus, Rowland Hill Street, London NW3 2PF, United Kingdom

[‡]Department of Food Science, Faculty of Agriculture, University of Naples Federico II, via Universitá 100, Parco Gussone, 80055 Portici, Italy

Abstract

We have used a proteomics subcellular spatial razor approach to look at changes in total protein abundance and in protein distribution between the nucleus and cytoplasm following exposure of MCF7 breast cancer cells to estradiol. The dominant response of MCF7 cells to estrogen stimulation involves dynamic changes in protein subcellular spatial distribution rather than changes in total protein abundance. Of the 3604 quantitatively monitored proteins, only about 2% show substantial changes in total abundance (>2-fold), whereas about 20% of the proteins show substantial changes in local abundance and/or redistribution of their subcellular location, with up to 16-fold changes in their local concentration in the nucleus or the cytoplasm. We propose that dynamic redistribution of the subcellular location of multiple proteins in response to stimuli is a fundamental characteristic of cells and suggest that perturbation of cellular spatial control may be an important feature of cancer.

[*]Corresponding Author: (J.G.-Z.) j.godovac-zimmermann@ucl.ac.uk.

ASSOCIATED CONTENT

Supporting Information

Supplementary Table S1: Master table of MS data for all fractions and replicates. Supplementary Table S2: Summary of SILAC data for the 134 set of proteins. Supplementary Text: Mathematical formulation of the subcellular spatial razor. Supplementary Figure S1: Purity of the subcellular fractions and fluorescence imaging. This material is available free of charge via the Internet at http://pubs.acs.org.

The authors declare no competing financial interest.

Europe PMC Funders Author Manuscripts

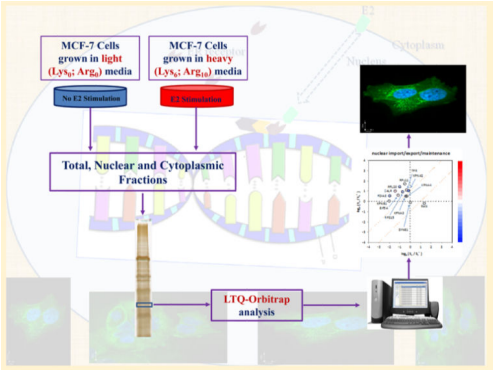

Keywords

Estrogen; MCF-7 cells; breast cancer; subcellular protein location; nucleus; cytoplasm; SILAC; quantitative proteomics; mass spectrometry; estrogen receptor; nuclear hormone receptors; protein trafficking

1. INTRODUCTION

Despite scientific progress in diagnosis and treatment, breast cancer continues to be one of the main causes of death in women. Excluding hereditary predispositions to the onset of this disease, reproductive aspects, such as early menarche and late menopause or an advanced age at the first pregnancy, or behavioral aspects, such as the increased use of hormone replacement therapy, are factors positively correlated to a higher risk of breast cancer occurrence, and all of these factors involve a more prolonged exposure to sex hormones, primarily estrogens.[1,2] Extended exposure to exogenous or endogenous damaging agents causes an accumulation of irreversible abnormalities in the genome and epigenome that reprogram the cell to accelerate growth and to inhibit its death. Many investigations at the cellular level have been based on measuring gene expression of breast cancer cells using transcriptomic and molecular biology techniques. There are important reasons[3,4] to complement this work with high throughput proteomics methods to obtain in-depth understanding of the molecular basis of cancer. These include that protein abundance may be different than transcript abundance and that for genetic variation, translation and protein stability may be more determinant for protein abundance than transcript levels.[5] At the same time, very complex cellular signaling systems modulate cancer cell function through post-translational modifications such as phosphorylation[6] and methylation/acetylation.[7,8] An emerging theme is that the subcellular distribution of proteins[9,10] and other molecules such as tRNA[11] is dynamic and context-dependent and that proteins may have different functional roles at different subcellular locations.[12-14] For MCF-7 (Michigan Cancer Foundation-7) cells, at least 50% and perhaps as much as 75% of proteins have been demonstrated to have multiple subcellular locations.[15] About 1000 proteins have been shown to be present in both the nucleus and mitochondria of MCF-7 cells and many of these proteins are known to have different function in the two subcellular locations.[16] Massive changes in the spatiotemporal subcellular distribution of proteins have been detected in many cell types in response to a variety of factors including environmental stress, cell-cycle

signals, growth factors, and hormone exposure.[17] The importance of nucleo-cytoplasmic trafficking of BRCA1 in hereditary forms of breast cancer[18] is well-known. Given these emerging themes, the present work presents a high throughput proteomics study of the redistribution of proteins between the nuclear and cytoplasmic compartments of MCF-7 breast cancer cells when exposed to estradiol.

The effects on breast cancer cells of stimulation with estradiol (notably, 17*β*-estradiol, E2) have been widely studied. The sole addition of E2 induced proliferation of serum-starved MCF-7 cells and the mitogenic response to E2 was correlated to the MCF-7 strain.[19] Moreover, cell stimulation with E2 has been reported to cause the proliferation of MCF-7 cells, but to induce apoptosis in MCF-7:5C cells.[20] In its role as a potent proliferation stimulator in responsive cells, estrogen can indirectly stimulate glycolysis and directly increase the glucose consumption rate through the regulation of glucose transporter 1 (GLUT1) expression[21] or of the catalytic activity of glyceraldehyde-3-phosphate dehydrogenase (GAPDH).[22] Overexpression of the glycolytic enzymes, fructose-1,6-bi-sphosphatases FBP1 and FBP2, as well as of known estrogen-regulated proteins such as PGR, TFF1, GREB1, TPD52L1, and TFRC, has been detected by proteomics in MCF-7 cells stimulated with 10 nM E2.[23]

It is well-known that the biological effects of E2 are mainly mediated by estrogen receptors (ERs).[24,25] Binding of estrogen to ERs causes conformational changes in the receptors, leading to dissociation of heat-shock chaperone proteins and to formation of stable receptor dimers.[26] These dimers recognize their cognate response element (ERE) within the regulatory region of the target genes[27] and are able to modulate the gene expression of cells, activating or suppressing the transcription of a target gene in a promotional and cell-specific manner,[28] and to induce directly the expression of cell cycle regulatory genes.[29,30] Interestingly, in addition to effects on transcription, bound E2 regulates ER abundance by considerably decreasing its half-life to 3–5 h.[31] Indeed, ER is preferentially ubiquitinated in the presence of E2 and the ER-hormone complex is degraded by a cytoplasmic fraction of the proteasome system.[32,33] Apart from transcriptional activities, ER receptors have other activities in the cytoplasm, mitochondria, and at the plasma membrane, and dynamic subcellular trafficking of ER receptors and other proteins appears to be essential to the properties of ER-related functional networks.[34-36]

We have recently developed high-throughput proteomics methods suitable for investigating dynamic aspects of protein subcellular distribution in the response of cells to stimulations.[10] This approach, which combines global quantitative proteomics with the analysis of fractions enriched in target subcellular locations, has allowed measurement of the changes in total abundance and in the compartmental abundance/distribution between the nucleus and cytoplasm for several thousand proteins differentially expressed in MCF-7 cells in response to estrogen stimulation. The development of a subcellular spatial razor model of the dynamic redistribution of proteins has facilitated the interpretation of large data sets obtained by the combination of stable isotope labeling in cell culture (SILAC) and of high-resolution mass spectrometry analysis. The present results show that as a consequence of estradiol stimulation of MCF-7 cells, massive numbers of proteins redistribute between the nucleus and cytoplasm and that many more proteins show appreciable changes in

compartmental abundance than in total protein abundance. We suggest that major alterations in the spatiotemporal subcellular distribution of proteins are the dominant response of MCF-7 cells to estradiol exposure, that a major role of the estrogen receptor and possibly other nuclear hormone receptors may be the polling of and response to spatially distributed functional networks, and that strong perturbation of subcellular spatial regulation may be a crucial feature of breast cancer.

2. MATERIALS AND METHODS

2.1. Cell Culture and SILAC Labeling

MCF-7 cells were purchased from the ATCC (HTB-22, Manassas, VA) and cultured in a humidified incubator at 37 °C with 5% CO_2 in SILAC DMEM-Flex media (Invitrogen, Paisley, U.K.), supplemented with 10% dialyzed fetal bovine serum (FBS, Invitrogen), 100 U/mL of penicillin, and 100 μg/mL of streptomycin (Gibco, Invitrogen). For SILAC analysis of two isotope labels, the cells were divided into two populations, labeled with either "light" (L-lysine-2HCl and L-arginine-HCl) or "heavy" (L-lysine-2HCl, $^{13}C_6$ and L-arginine-HCl, $^{13}C_6$, $^{15}N_4$) media (Invitrogen, Paisley, U.K.) and cultured for six passages in order to achieve full incorporation of the SILAC amino acids.

2.2. Cell Treatment

MCF-7 cells were grown in heavy and light SILAC medium. After six doublings, full incorporation of labels into the cells was checked by MS analysis of samples. After the cells reached 70–80% confluence, SILAC medium supplemented with 10% dialyzed FBS was replaced with the same SILAC medium without phenol red and grown for 48 h prior to E2 treatment. Cells growing in heavy SILAC medium were subsequently stimulated with estradiol (10 nM final concentration) for 24 h, while the light cells were kept in phenol-free medium for a further 24 h.

2.3. Sample Preparation

As summarized below, the preparation of total, nuclear, and cytoplasmic samples largely followed our previous procedures.[16] Three replicates were prepared by parallel breakage and fractionation of three aliquots of the labeled cells.

Cells were washed three times within tissue culture flasks with cold phosphate buffer saline (PBS) in order to remove most of the FBS and centrifuged at 300*g* for 5 min. All of the following steps for organelle separation were performed at 4 °C in the presence of protease and phosphatase inhibitor cocktails. One pellet for each light and heavy cell culture was in parallel dissolved in cold RIPA lysis buffer (50 mM Tris-HCL at pH 7.5, 300 mM NaCl, 1% NP40, 0.5% sodium deoxycholate, 0.1% SDS, and 1 mM EDTA), agitated for 20 min at 4 °C, and centrifuged at 300*g* for 5 min (Heraeus Biofuge Pico, Thermo Fisher Scientific, U.K.). The supernatant fraction contained the total lysate sample (T). For subcellular fractionation, another pellet for each light and heavy cell culture was suspended in a cold hypotonic osmotic buffer (10 mM NaCl, 1.5 mM $MgCl_2$, and 10 mM Tris-HCl at pH 7.4), by vortex mixing and left to swell on ice for 10 min. After centrifugation at 100*g* for 10 min, the breaking buffer was added to the pellet containing 300 mM sucrose, 1 mM EDTA, 5

U/mL of heparin, 10 mM HEPES, and 5 mM $MgCl_2$ at pH 7.4. Cells were broken gently by liquid shear in a tight-fitting glass Dounce homogenizer (0.05–0.08 mm clearance), and the cell suspension was centrifuged for 10 min at 800*g* in order to obtain the nuclear pellet, while the supernatant was kept for isolation of the cytoplasmic fractions.

For nuclear-enriched (N) fractions, the nuclear pellet was suspended in a hypotonic buffer containing 10 mM HEPES at pH 7.9, 10 mM KCl, 5 mM $MgCl_2$, 2 mM EDTA, 1 mM dithiothreitol (DTT), and 0.1% Triton X-100 and incubated for 15 min at 4 °C on a rotating platform. Nuclei were spun down and extracted with high salt breaking buffer containing 20 mM HEPES at pH 7.9, 700 mM NaCl, 1.5 mM $MgCl_2$, 1 mM EDTA, and 10% glycerol for 2 h at 4 °C on a rotating platform. The extract was centrifuged for 10 min at 800*g* to remove any residual cell debris. The supernatant, subjected to acetone precipitation by adding four volumes of 80% acetone, was left for a minimum of 1 h, at −20 °C, and then spun down at 16000*g* for 30 min at 4 °C. The pellet was air-dried and resuspended in a 1× protein solubilization buffer, 20 mM PIPES at pH 7.3, 300 mM NaCl, 2% Triton X-100, 0.2% SDS, and 2% sodium deoxycholate.

For the cytoplasmic-enriched (C) fractions, an equal volume of dilution buffer (1 mM EDTA, 5 U/mL of heparin, 10 mM, HEPES, and 5 mM $MgCl_2$ at pH 7.4) was added to supernatant and centrifuged for 30 min at 22000*g* in an Optima TLX ultracentrifuge (Beckman Coulter, Fullerton, CA). The pellet was resuspended in a 1× protein solubilization buffer (20 mM PIPES at pH 7.3, 300 mM NaCl, 2% Triton X-100, 0.2% SDS, and 2% sodium deoxycholate). The supernatant was subjected to acetone precipitation as described above, the pellet resuspended in a 1× protein solubilization buffer and kept as the cytoplasmic-enriched (C) fraction.

2.4. Fractionation Tests by Western Blotting Analysis

To routinely assess the fractionation quality, Western blotting analysis of two constitutive proteins was carried out, VDAC, to track the location of mitochondrial proteins enriched in the cytoplasm fraction, and Histone H3, for nucleus fraction.

Twenty micrograms of each sample (total lysate, cytoplasm, and nuclear fractions) were electrophoretically resolved by 12% SDS-PAGE. The resulting gels were transferred to a PVDF membrane using a Mini trans-blot cell and Powerpac basic power supply (BioRad, Herts, U.K.) at a constant 100 V/350 mA. After 1 h, the blots were blocked with 5% milk–TBS–Tween saline buffer (TBST: 20 mM Tris buffer, 150 mM NaCl, and 0.1% Tween-20, pH = 7.5) for 2 h at 4 °C under slow agitation, followed by a rinse for 5 s in TBST. The membranes were incubated overnight at 4 °C with 2 different primary antibodies: anti-VDAC (ab34726, Abcam, Cambridge, U.K.) and anti-Histone H3 (ab1791, Abcam), at 1:1000 and 1:2500 dilutions, respectively. After washing the membranes with TBST three times (10 min for each washing) under agitation, the membranes were incubated for 1 h with a secondary antibody conjugated to horseradish peroxidase (#7074, Cell Signaling Technology, New England BioLabs, Hitchin, U.K.) at a dilution of 1:1000 for VDAC and 1:5000 for H3. The membranes were washed three times with TBST (10 min for each wash) and with TBS for 5 min, under agitation. Finally, proteins were visualized using

chemiluminescence reagents ECL Plus and Hyper Film (GE Healthcare, Bucks, U.K.) and a Xograph imaging system Compact ×4 (Xograph Healthcare, Stonehouse, U.K.).

2.5. In-Gel Protein Digestion

The protein concentration of all the samples was evaluated with the Bio-Rad protein assay kit (Bio-Rad, Hemel Hempstead, UK). For comparative SILAC analysis, heavy and light total cell lysates and nuclear and cytoplasmic fractions were mixed in a 1:1 ratio based on the final protein concentration (30 μg) and separated by 12% SDS-PAGE, under reducing conditions. Proteins were visualized by silver staining (ProteoSilver Plus, Sigma Aldrich, Poole, U.K.), and bands (33 horizontal slices), excised from the gel lane, were destained using a solution containing 100 mM sodium thiosulphate and 30 mM potassium ferricyanide in ratio 1:1. Samples were reduced by 10 mM DTT and alkylated with 100 mM iodoacetamide using the ProGest Investigator Instrument (DigiLab, Genomics Solutions, Cambs, U.K.) according to the established protocol.[37] Finally, each dry gel piece was rehydrated in 30 μL of 50 mM ammonium bicarbonate solution containing 250 ng of Trypsin Gold, Mass Spectrometry grade (Promega, Madison, USA), and incubated at 37 °C overnight. The trypsinolysis was stopped with 0.1% formic acid (FA), and tryptic peptides were eluted, vacuum-dried, and dissolved in 0.1% formic acid for LC–MS/MS analysis.

2.6. Mass Spectrometry

LC–MS/MS analysis was performed with an LTQ-Velos mass spectrometer (Thermo Fisher Scientific). Peptide samples were loaded using a Nanoacquity UPLC (Waters, U.K.) with Symmetry C18 180 μm × 20 mm (Waters part number 186006527) trapping column for desalting and then introduced into the MS via a fused silica capillary column (100 μm i.d.; 360 μm o.d.; 15 cm length; 5 μm C18 particles, Nikkyo Technos CO, Tokyo, Japan) and a nanoelectrospray ion source at a flow rate at 0.42 μL/min. The mobile phase comprised H_2O with 0.1% formic acid (buffer A) and 100% acetonitrile with 0.1% formic acid (buffer B). The gradient ranged from 1% to 30% buffer B in 95 min followed by 30% to 60% B in 15 min and a step gradient to 80% B for 5 min with a flow of 0.42 μL/min. The full scan precursor MS spectra (400–1600 m/z) were acquired in the Velos-Orbitrap analyzer with a resolution of r = 60 000. This was followed by data dependent MS/MS fragmentation in centroid mode of the most intense ion from the survey scan using collision induced dissociation (CID) in the linear ion trap: normalized collision energy 35%; activation Q 0.25; electrospray voltage 1.4 kV; capillary temperature 200 °C; and isolation width 2.00. The targeted ions were dynamically excluded for 30 s, and this MS/MS scan event was repeated for the top 20 peaks in the MS survey scan. Singly charged ions were excluded from the MS/MS analysis, and XCalibur software version 2.0.7 (Thermo Fisher Scientific, U.K.) was used for data acquisition.

2.7. Protein Identification and Quantification

Raw MS files from the three technical replicates for SILAC total, nucleus, and cytoplasm experiments were automatically assembled by MaxQuant (version 1.3.0.5) and visualized by Perseus (version 1.3.0.4) software platform. A matrix of SILAC ratios with rows corresponding to proteins and columns to different samples or conditions was automatically

assembled by MaxQuant software and cross-experiment protein ratios were successfully compared for the quantification of SILAC pairs, identification of individual peptides, and assembly into protein groups.[38,39] The derived peak list generated by Quant.exe (the first part of MaxQuant) was searched using the Andromeda search engine against human FASTA files (HUMAN.fasta.gz) obtained from the UNIPROT Web site: ftp://ftp.uniprot.org/pub/databases/uniprot/current_release/knowledgebase/proteomes, last modified 5/10/2012. Selected parameters for Max-Quant analysis included the trypsin enzyme specificity and 2 missed tryptic cleavages, oxidation of methionine and acetylation of protein N-terminal as variable modifications and cysteine carbamidomethylation as a fixed modification. SILAC doublet measurements of Lys_6 and Arg_{10}, minimum peptide length of 6 amino acids, minimum of 1 peptide, minimum of 1 razor + unique peptide and minimum 1 of unique peptide, top 6 MS/MS peaks per 100 Da, peptide mass tolerance of 10 ppm for precursor ions, and MS/MS tolerance of 0.5 Da. All proteins were filtered according to a false discovery rate (FDR) of 0.01% applied at both peptide and protein levels and a maximum peptide posterior error probability (PEP) of 1. Proteins were automatically quantified in the MaxQuant software: a minimum of 2 peptide ratio counts from razor and unique peptides were necessary for protein quantification, thus permitting requantification as an option. An experimental design template was used to specify individual replicate experiments (each data set contained three technical replicates) and reverse labeling conditions within the analysis. MaxQuant output files were subsequently uploaded into Perseus in order to calculate the Significance B scores as well as the GO term association for each protein group.

2.8. Correlation and Quantitation of Proteins Across Samples

The MaxQuant software package[38,39] was used to identify and quantify proteins for 16 analysis sets: (a) each nucleus (N) sample replicate and the union of the three N samples, (b) each cytoplasm (C) sample replicate and the union of the three C samples, (c) each total (T) sample and the union of the three T samples, and (d) each C&N replicate and the union of the three C&N samples. C&N denotes that, for each individual replicate, the MS data for the C and N samples were jointly processed with MaxQuant to estimate changes in total protein abundance. For this data, a correction for enrichment of nuclear proteins in the MS data collection was applied during estimation of total protein abundance (see Supporting Information). Because slightly different protein sequence groups from the same underlying gene were sometimes observed for the different samples as a consequence of the exact set of peptides detected in each data set, we also jointly processed all 9 MS data sets (a C&N&T data set) to correlate the protein sequence groups across the 16 analysis sets. Across all samples, a total of 4386 different proteins were identified by sequenced peptides. Of these, 110 corresponded to 55 proteins with multiple isoforms from the same gene that could not be unambiguously resolved across all replicates of the three sample types and were not further analyzed for present purposes. Supplementary Table S1 contains the full experimental data for the remaining 4276 proteins.

2.9. Confocal Fluorescence Imaging of Live Cells

MCF-7 cells were grown in DMEM-F12 medium on a 35 mm imaging dish with a glass bottom (WillCo-dish “Series GWSt-3512”, WillCo Wells, Amsterdam, The Netherlands).

Upon reaching 60% confluence, the cells were washed with PBS and incubated for 48 h with DMEM-F12 phenol red-free medium supplemented with 10% charcoal treated FBS, and medium was changed every 24 h before E2 stimulation. At the 48 h time point, cells were divided into two parts, nonstimulated (control) and stimulated with 10 nM E2 for further 24 h. After 24 h postestrogen stimulation, cells were washed twice in 1× PBS^+ (137 mM NaCl, 2.7 mM KCl, 10 mM $Na_2HPO_4{\cdot}2H_2O$, 1.8 mM KH_2PO_4, 1 mM $CaCl_2$, and 0.5 mM $MgCl_2{\cdot}\ 6H_2O$ at pH 7.4). For mitochondrial labeling, each dish of treated and untreated cells was incubated for 30 min with 20, 100, and 200 nM of MitoTracker Green (M7514 from Life Technology), in PBS^+ buffer, at 37 °C, 5% CO_2. Before respective nuclear labeling, cells were washed twice with PBS^+ buffer and then incubated with 1 μg/mL of Hoechst 33342 nuclear probe (R37605 from Life Technology), in dark at room temperature, for further 30 min. Prior to imaging, each dish was washed three times with PBS^+ buffer, and each wash was followed by incubation for five minutes at 37 °C in 5% CO_2. After the final wash, HEPES containing phenol red and serum-free medium was added to each dish to maintain alive cells during confocal imaging. Mitochondria and nucleus were visualized by confocal microscopy using fluorescence excitation (Ex) and emission (Em) of (490/516 nm) and (353/483 nm), respectively.

2.10. Immunofluorescence

Cells were grown in DMEM-F12 medium on glass coverslips (#1.5 thickness, 13 mm diameter) and treated as described in the live cell fluorescence microscopy section. Control (no E2 starvation/stimulation), unstimulated, and stimulated cells were then fixed in 4% paraformaldehyde for 10 min and permeabilized with a fresh 0.3% Triton X-100 solution in PBS for 5 min. After blocking with 5% BSA in PBS for 1 h at room temperature, the stimulated and unstimulated cells were both incubated overnight at 4 °C with anti-NQO1 (ab34173, Abcam) and Anti-PARK7/DJ1 antibody (ab76008, Abcam) diluted in 1% BSA in PBS according to the manufacturer's specifications. Secondary antibody (green) incubation was performed for 2 h at room temperature in the dark using goat Anti-Rabbit IgG H&L (DyLight 488) antibody (ab96899, abcam) diluted 1/250 in 1% BSA/PBS. Control coverslips were divided into two parts: a control-A labeled coverslip was incubated only with secondary antibody, while the control-B coverslip was incubated with both anti-PARK7/DJ1 and secondary antibodies. All coverslips were then stained with 1.43 μM of DAPI (D3571, Invitrogen) and incubated for 5 min at room temperature in dark. In all procedure, every step was followed by washing with PBS for 3 times. Finally, coverslips were mounted with Dako Fluorescent Mounting Medium. The immunofluorescence images were obtained with a Perkin-Elmer Ultraview Vox spinning disc confocal microscope equipped with ×63 Plan Apo (NA 1.4) oil immersion objective, and nuclei were visualized using Ex of 358 nm and Em of 461 nm.

3. RESULTS

The proteomics subcellular spatial razor experiments described in the following are based on a model that envisages that in response to a cellular perturbation, proteins may show both changes in total cellular abundance and in their subcellular spatial distribution between the nucleus and cytoplasm (Figure 1). Experimental measurements of protein abundance ratios

(SILAC ratios) between stimulated/unstimulated cells are made on three samples: (1) an unfractionated, total cell lysate (T), (2) a nucleus-enriched sample obtained by subcellular fractionation (N), and (3) the corresponding nucleus-depleted sample (C), which we refer to as the cytoplasm in the following text. The corresponding SILAC ratios provide measures for each protein of the overall change in total cellular abundance (S_t), or of the localized change in abundance in the nuclear (S_n) or cytoplasmic (S_c) subcellular compartments. A mathematical formulation of the model is given in the Supporting Information. Stringent purification of organelles (e.g., nucleus) was not attempted in this study as we believe it is not feasible to purify to homogeneity organelles that are subject to dynamic changes in their protein content and that unnecessary protein loss is incurred during such organelle isolation methods. We preferred to use highly enriched fractions rather than highly purified organelles; this is a strategy that has previously been shown to successfully detect nucleo-cytoplasmic trafficking.[10]

We have previously characterized in detail samples obtained with the present subcellular fractionation protocols, including extensive evidence that the nuclear-enriched fraction contains very little if any contamination with other cytoplasmic components such as mitochondria, endoplasmic reticulum, Golgi apparatus, etc.[16] As routine controls for the present preparations, we checked the morphology of stimulated/unstimulated cells using fluorescence imaging to verify the absence of nuclear breakage and checked the purity of the nuclear/cytoplasmic fractions using Western blotting (Supplementary Figure S1). For each sample type, we measured three replicates. Across all samples, a total of 4386 different proteins were identified by sequenced peptides. Of these, 110 corresponded to 55 proteins with multiple isoforms from the same gene that could not be unambiguously resolved across all replicates of the three sample types and were not further analyzed for present purposes. Supplementary Table S1 contains the full experimental data for the remaining 4276 proteins. For quantitative analysis of the distribution of the subcellular abundance of these proteins, we imposed the conservative limits that at least two different sequenced peptides (1 unique) and at least 3 SILAC ratio counts in a single sample replicate were required. This gave 3604 quantified, reliably identified proteins, with the subcellular distribution shown in Figure 2, that were used in the analyses described below.

3.1. Changes in Abundance in the Nuclear and Cytoplasmic Compartments

The overall changes in abundance for the proteins are shown in Figure 3. For 2809 total lysate (T) proteins with ≥5 SILAC ratio counts across the three replicates (median of 39 counts per protein), only 7 T proteins (0.2%) showed greater than 4-fold increase/decrease in abundance and only 64 T proteins (2.3%) showed greater than 2-fold increase/decrease in abundance in response to estradiol exposure (Figure 3A). To check for possible distortion of the distribution profile by lower abundance proteins and/or by variation between replicates, these results were compared with a smaller set of 2197 more abundant proteins for which the lower limit was set to ≥3 SILAC ratio counts in all three T replicates (median of 62 counts per protein, Figure 3B). The profile for the distribution of the SILAC ratio S_t for total cellular proteins was hardly changed, which indicates that it is a reliable indicator of total cellular abundance changes.

In the nuclear compartment, very different behavior was observed (Figure 3A). For 1791 nuclear proteins with ≥5 SILAC ratio counts across the three replicates (median of 22 counts per protein), only 2 proteins (0.2%) showed greater than 2-fold increase in nuclear abundance. However, 109 proteins (6.1%) showed greater than 4-fold decrease and 560 proteins (31.3%) showed greater than 2-fold decrease in nuclear abundance. For 1064 more abundant nuclear proteins with ≥3 SILAC ratio counts in all three N replicates (median of 49 counts per protein), a similar distribution profile for the SILAC ratio S_n for nuclear proteins indicated that lower abundance proteins and/or variation between replicates had little effect on the observed distribution (Figure 3B).

For cytoplasmic proteins, largely inverse changes were observed. For 1758 cytoplasmic proteins with ≥5 SILAC ratio counts across the three replicates (median of 39 counts per protein), 21 (1.2%)/130 (7.4%) of proteins showed greater than 4-fold/2-fold decreases in cytoplasmic abundance, but 65 (3.7%)/407 (23.2%) of the proteins showed greater than 4-fold/2-fold increases in cytoplasmic abundance. Exclusion of lower abundance proteins by requiring ≥3 SILAC ratio counts in all C replicates (median of 54 counts per protein) caused only very modest change in the distribution profile for the SILAC ratio S_c for cytoplasmic protein abundance (Figure 3B).

3.2. Coupling between Total and Compartmental Changes in Abundance

Because the abundance of a protein in the nucleus/cytoplasm can be altered by changes both in total cellular protein abundance and in distribution between the two compartments, the SILAC ratios S_n and S_c do not directly measure redistribution of a protein between the two compartments. If f_s and f_u denote the fraction of a protein in the nucleus in stimulated/unstimulated cells, respectively, then $S_n/S_c = f_s(1 - f_u)/f_u(1 - f_s)$ provides a direct measure for redistribution to/from the nucleus (see Supporting Information). We directly tested for correlation between total and compartmental changes in abundance by plotting S_n/S_c vs S_t for 724 abundant proteins that had ≥3 SILAC ratio counts for all three C, N, and T replicates (median of 307 counts per protein, Figure 4a). A total of 424 proteins showed $|\log_2(S_n/S_c)| > 1$ and/or $|\log_2(S_t)| > 1$. However, there was no apparent correlation between overall changes in abundance (S_t) and changes in subcellular distribution (S_n/S_c), that is, the abundance changes in the nuclear and cytoplasmic compartments do not simply mirror changes in total abundance. It should be noted that the distribution profiles for S_t and S_n/S_c show good reproducibility over the three biological replicates (Figure 4B,C). Although there tends to be more scatter for major changes in distribution that involve residual fractions of a protein in one of the compartments, i.e., $\log_2(S_n/S_c) \lesssim -2$, the trafficking of the respective proteins is clear (see below). The strong skewing of $\log_2(S_n/S_c)$ to negative values (Figure 4C) reflects predominant N → C subcellular redistribution.

To further characterize the nature of the redistribution for individual proteins, we used the full 3D model of the subcellular spatial razor. For the 3D space of measured parameters $\{S_n, S_c, S_t\}$, the orthogonal basis set $\{S_c/S_t, S_n/S_t, S_t\}$ separates an axis with changes in total protein abundance (S_t) from a plane (S_c/S_t, S_n/S_t) that depends only on the redistribution of a protein between the nucleus and cytoplasm (see Supporting Information). Figure 5B shows that in the distribution plane, the data points are constrained by conservation of mass (no

differential protein losses between stimulated/unstimulated samples during subcellular fractionation or MS sample preparation) to lie in 2 quadrants that correspond to N → C or N ← C redistribution of the protein, respectively. Figure 5A,C shows typical behavior for 6 proteins from Figure 4A. In the 3D space (Figure 5C), the changes in total abundance, perpendicular to the distribution plane, have been color-coded for the average over the 3 replicates.

The locations of the data points in the distribution plane (Figure 5C) are sensitive to the basal nucleus/cytoplasm distribution of the protein in unstimulated cells. For example, NHP2L1 corresponds to a protein with an abundance distribution strongly skewed to the nucleus. Upon stimulation the nuclear/total abundance is hardly changed ($\log_2(S_n) \approx \log_2(S_t) \approx 0.03$), but the small fraction of the protein in the cytoplasm is increased 6-fold. This might be the behavior of a protein involved in transmission from the nucleus to the cytoplasm of information about cellular state. Conversely, upon exposure to estradiol the abundance of CASP14 decreased 3-fold, with little or no change in subcellular distribution. ERP29, AGR3, and EZR represent proteins with strong basal distribution to the cytoplasm. ERP29 and AGR3 both show 2-fold increases in total abundance, accompanied by enhanced depletion of the protein in the nucleus. These might be proteins that transmit information about cellular state from the cytoplasm to the nucleus, or this might even reflect negative regulation of their own abundance. EZR shows a moderate decrease in abundance (S_t = 0.71), but this is preferentially in the cytoplasm and leads to a 2-fold increase in the fraction of the protein in the nucleus. Finally, SUB1 (PC4) represents a protein with very little change in total abundance (S_t = 1.02), but substantial, coupled changes in abundance in the two compartments (S_n = 1.56; S_c = 0.48). Note that in the 3D space the distribution plane is sensitive to changes in the fractional abundance in both subcellular locations; even where this might, for example, represent an increase/decrease in the nucleus for a trace fraction of the total protein if the protein has a basal abundance strongly skewed to the cytoplasm (see Discussion). There is some scatter between the replicates (Figure 5). This together with the inherent precision of the SILAC measurements, especially of the ratios S_n/S_t or S_c/S_t for proteins with basal abundances strongly skewed to one location, can lead to minor apparent violations of conservation of mass and contributes to the scatter in Figure 4C for $\log_2(S_n/S_c) \lesssim -2$. However, in most cases the overall behavior of the proteins could be clearly ascertained.

There were appreciable numbers of proteins for which no substantial change in either abundance or subcellular location was detected (bounding box in Figure 4A), i.e., the effects of estradiol exposure seem to be selective. Only a handful of proteins showed appreciable changes in total abundance without changes in subcellular distribution (Figure 4A). Overall there was very little correlation between changes in total protein abundance and changes in protein abundance in the two subcellular compartments. For some individual proteins, initially counterintuitive results were detectable, e.g., AGR3 increases in total abundance but decreases in abundance in the nucleus (Figure 5C).

3.3. Redistribution of Proteins between the Nucleus and Cytoplasm

We expanded the analysis to proteins that were detected in only one compartment and screened for inadequate MS sampling and/or fractionation artifacts by using the fact that the spatial razor model explicitly includes conservation of mass. This provides a strong framework for screening experimental results for artifacts and obtaining a set of proteins with high confidence changes in compartmental abundance. For example, for proteins present in a single subcellular compartment, changes in abundance in that compartment are necessarily coupled by conservation of mass to changes in total abundance, i.e., $S_n/S_t = 1$ (nucleus) or $S_c/S_t = 1$ (cytoplasm). A similar principle applies to proteins present in both compartments: for ideal sampling and fractionation, joint coprocessing of the C and N MS data sets (a C&N data set) should give an apparent change in abundance S_t* such that S_t*/$S_t = 1$ (see Supporting Information). For the proteins which had at least 3 ratio counts in the appropriate samples and for which the ratio S/S_t could be calculated, all of these ratios showed a Gaussian distribution. Outliers represent proteins for which strict conservation of mass is less reliable due to reduced MS sampling and/or fractionation/extraction artifacts (see Supporting Information).

Of the 3604 proteins in our quantified set, a substantial majority (2597) was detected in more than one sample. However, most such proteins were detected in the CNT subset (1683): only 217/598 proteins were included in the CT/NT subsets, and only 160/374 were quantified in both samples. For those single-compartment proteins with good consistency with conservation of mass, the table in Figure 6 shows that there were very few proteins with >2-fold changes in abundance. Although the total number of quantified single-compartment proteins is small, the results are consistent with the observation that, of 3057 quantified T proteins, only 71 (2.3%) showed >2-fold changes in total abundance.

For the 1363 proteins quantified in all three samples of the CNT data subset, the table in Figure 6 shows how the proportion of proteins with appreciable changes in total abundance (S_t), compartmental abundance (S_c, S_n), or redistribution (S_n/S_c) varies with the range of inclusion relative to the center of the Gaussian distribution for S_t*/S_t. There were no proteins for which the nuclear abundance doubled; only 8 proteins (~1.3%) for which cytoplasmic abundance was halved and only 5 proteins (~1%) for which there was a 2-fold change in total abundance. In contrast, ~14% of cytoplasmic proteins showed doubled abundance, and ~30% of nuclear proteins showed halved abundance. About 50% of the proteins showed $|\log_2(S_n/S_c)| > 1$. These percentages were largely independent of the total number of proteins included in the conservation of mass selection range around S_t*/$S_t = 1$ (Figure 6).

The behavior of the individual proteins is shown in Figure 6A. Overall, with $|\log_2(S_t*/S_t)| < 0.5$, the CNT data set included 331 proteins that showed >2-fold change in at least one of the SILAC ratios S_n, S_c, S_t, or S_n/S_c. Only 5 proteins showed >2-fold change in S_t, and only for CASP14 did the >2-fold decrease in total abundance result in corresponding >2-fold decreases in both the nuclear and cytoplasmic compartments. For the other proteins that showed >2-fold increase/decrease in total abundance (TUFM, AGR3/BASP1, and ACBD3), redistribution resulted in a >2-fold change in only one of the nuclear/cytoplasmic compartments. For 326 proteins, there were >2-fold changes in S_n, S_c, or S_n/S_c without a >2-

fold change in S_t. There were 166 proteins that showed a >2-fold decrease in abundance only in the nucleus, but none that showed a >2-fold increase only in nuclear abundance. There were 83 proteins that showed >2-fold changes in abundance only in the cytoplasm, 77 of which were increased abundance. A >2-fold decrease in abundance in the nucleus coupled with a >2-fold increase in the cytoplasm was detected for 10 proteins. Finally, there were 67 proteins that showed substantial redistribution between the N and C compartments without a 2-fold change in either compartment, e.g., for PSME3, $S_c = 1.83$; $S_n = 0.64$; $S_n/S_c = 0.35$.

To test the robustness of the distribution over the five classes of proteins shown in Figure 6A, we extracted a set of 134 proteins for which a 2-fold variation in one or more of S_n, S_c, S_t, or S_n/S_c was obtained for at least 2 replicates, with at least 10 SILAC ratio counts in each replicate (Figure 6B, median of 549 ratio counts per protein). A summary of the data for these proteins is given in Supplementary Table S2. The distribution over the five classes showed at most modest changes (Figure 6A,B), and we therefore take this distribution as characteristic of the response of MCF7 cells to estradiol. For Protein DJ-1 (PARK7), which showed $S_n = 0.25$ (Supplementary Table S2), we confirmed the large reduction in nuclear abundance for unbroken cells using immunofluorescence imaging (Supplementary Figure S1).

Notable was that in all of the above data subsets there were very much larger numbers of proteins that showed >2-fold changes in compartmental abundance compared to those with >2-fold changes in total abundance. The functional significance of this data is considered further below and in the discussion. From the proteins in the CT, NT, and CNT data sets that showed good consistency with conservation of mass, the 134 set of abundant proteins was used to investigate possible correlations with database/literature information on subcellular location, functional processes, involvement of nuclear import/export proteins, and partitioning of proteins between the nucleus and mitochondria (see below).

3.4. Subcellular Location Annotation for Proteins with Compartmentalized Abundance Changes

For the 134 set of proteins, we analyzed their current GO CC (cell component) annotation terms. The complete set of 733 annotations to 152 GO CC terms is given in Supplementary Table S2. Table 1 shows the distribution of the current annotations over four main top-level cellular locations (nucleus, cytoplasm, plasma membrane, and extracellular region), with a further breakdown of cytoplasmic locations. There was no subcellular location annotation for 5 of the 134 proteins. With the vocabulary of Table 1, the remaining 129 proteins had an average of 2.7 locations per protein, and a maximum of 6 locations, i.e., many of these proteins are known to have multiple subcellular locations. For example, of the 66 proteins currently annotated to the nucleus, 58 are also annotated to the cytoplasm (Table 1). Of the 120 proteins currently annotated to the cytoplasm, 58 are also annotated to the nucleus and 25 to the plasma membrane. This is consistent with the concepts that protein spatial location and organelle composition are dynamic properties that depend on context and that protein function is intimately coupled to subcellular spatial distribution.

However, we detected 76 proteins in both the cytoplasm and nucleus that have not previously been annotated to nucleus and 14 proteins in both the cytoplasm and nucleus that have not previously been annotated to cytoplasm. These results are consistent with previous studies indicating that current subcellular annotations in the GO CC database underestimate the dispersion of proteins over multiple locations in MCF7 cells[15,16] and suggest that coupling of cellular function to protein spatial distribution is even more prevalent than is implicit in current subcellular location annotations (see Discussion).

In this context, we recently identified 985 proteins that are present in both the nucleus and mitochondria of MCF7 cells.[16] With the greater number of MS replicates used in the present study, 1069 proteins that were previously detected in mitochondria[16] were detected in the nucleus in the present samples. This included confirmation of the unexpected presence in the nucleus of mitochondrial respiratory chain proteins and of many other metabolically interesting proteins such as pyruvate decarboxylase (PC) and mitochondrial phosphoenolpyruvate carboxykinase (PCK2).[16] At the level of at least 2 peptides and 3 SILAC ratio counts, 829 of these proteins were quantified in both the nucleus and cytoplasm in the present experiments. Following estradiol exposure, N → C redistribution involving >2-fold reduction in nuclear abundance was detected for 249 of these proteins. The 134-set of proteins showing the most reliable changes contained 87 of these proteins, which are included in the functional analysis below. While possible redistribution of these proteins to/from mitochondria will have to be confirmed by additional experiments, this suggests that dynamic subcellular protein distribution may have a major role in communication/coordination between the nucleus and mitochondria.

3.5. Functional Processes associated with Proteins Showing Compartmentalized Abundance Changes

For the 134 set of proteins, we used the Reactome software programs[40,41] to search for associated functional processes (Table 2). Our goal was to test whether the sets of redistributed proteins are likely to have important functional consequences and to obtain a qualitative appraisal of what kinds of processes might be involved rather than to specify exact functions. For example, all 5 proteins involved in glycolysis (a cytoplasmic process) show N → C redistribution involving >2-fold reductions in their nuclear abundance with no appreciable change in their cytoplasmic abundance (Table 2). This should not be interpreted as evidence for glycolysis in the nucleus, but rather as an indication for cross-talk between glycolysis and unknown nuclear process(es) that are influenced by estradiol exposure. Similarly, the Reactome *p*-value can only be moderately indicative since it is normalized to the proportion of all glycolytic proteins and does not assess the significance of redistribution of multiple glycolytic proteins to a wrong location differing from the cytoplasm.

With these kinds of caveats in mind, Table 2 nonetheless suggests that exposure to estradiol leads to changes in protein distribution that reflect processes over a wide spectrum of functions/subcellular locations. Because of substantial, different skewing in the basal, nonstimulated distribution of the various proteins between the nucleus and the cytoplasm, only some of the redistribution patterns shown for the functions in Table 2 are easily interpreted. For example, all 7 subunits of the CCT complex involved in chaperone-assisted

protein folding show >2-fold reductions in nuclear abundance, suggesting that this complex might be involved in protein import/export/folding in the nucleus (see Discussion). Similarly, all 5 proteins involved in nucleosome assembly show >2-fold increases in cytoplasmic abundance, with very minor changes in their nuclear and total abundance, suggesting this group might reflect signaling to the cytoplasm about a nuclear process. Seven proteasome subunits (see protein degradation in the cytoplasm section of Table 2) figure prominently in the functional groups in Table 2. Proteasomes occur in both the nucleus and cytoplasm, and the distribution pattern includes 4 proteins that show substantial redistribution without 2-fold changes in abundance in either compartment. We suggest that this type of redistribution pattern may reflect balancing of multiple functions between the nucleus and cytoplasm (see Discussion). Other functional groups show more complex redistribution patterns that may reflect wide functional cross-talk that is coupled to basal skewing of abundance over cellular location. This was the case for the plasma membrane functional groups, where it was intriguing to see indications for functions associated with actin-related processes in phagosome formation and for neuronal migration (L1CAM interactions). As with glycolysis, such groupings might reflect cross-talk with nuclear processes. For example, nuclear actin imported via importin-9 supports transcription[42] and myosin isoforms show directed, Ca^{2+}-dependent nuclear import.[43]

3.6. Proteins Involved in Nuclear Import/Export

With at least 5 ratio counts in the C, N, and T samples, there were 13 quantified proteins (median of 185 ratio counts per protein) in the full data set that have GO annotation corresponding to nuclear import/export/localization/maintenance (Figure 7). These proteins showed at most modest changes in total abundance (S_t = 1.19 CALR; 0.65 KPNA2) and essentially no change for RAN or KPNB1. In general, this subgroup of proteins showed a similar pattern to the overall set of quantified proteins, i.e., a trend of N → C redistribution following estrogen stimulation, with RAN as the only exception. There is little indication for general impairment of nuclear import/export. Indeed, the asymmetric distribution of RAN and karyopherins required for nuclear import is if anything enhanced.

4. DISCUSSION

Overall, the present results indicate that substantial changes in protein abundance in the nuclear/cytoplasmic compartments are observed for about ten times more proteins than those that show large changes in total cellular abundance. In short, the dominant consequence of the exposure of MCF7 cells to estradiol seems to be extensive redistribution of the compartmentalized subcellular abundance of the proteins rather than changes in their total abundance. In the following, we discuss three topics: (1) the suitability of the subcellular spatial razor for analysis of this dominant cellular response, (2) the role of dynamic protein subcellular distribution in the integration of cellular functional processes, especially in relationship to nuclear hormone receptors, and (3) possible implications for cancer.

4.1. Cellular Function and the Properties of the Spatial Razor

The present results show a strong preponderance in the number of proteins with appreciable N → C redistribution following exposure of MCF7 cells to estradiol. It is important to

emphasize that this does not imply that the total mass of nuclear proteins is dramatically decreased, and in fact, the present results could still be consistent with an increase in the total mass of nuclear proteins. This is because the individual proteins have very different cellular abundances and very different basal skewing between the nucleus and cytoplasm. Qualitatively, four major classes of proteins can be distinguished in the present results (Figure 6). (a) Proteins with appreciable changes in total abundance without redistribution of the fractions in the nucleus/cytoplasm. The present results suggest that such proteins are a minor contributor to the cellular response. (b) Proteins that show appreciable decrease in abundance only in the nucleus. This was the dominant class in the present study, but a large majority of such proteins show very limited change in cytoplasmic abundance (Figure 6), i.e., small proportions of cytoplasmic proteins present in the nucleus are expelled following exposure to estradiol. (c) Proteins that show appreciable increases in abundance only in the cytoplasm were another major group (Figure 6). Many of these proteins show limited change in abundance in the nucleus, i.e., small proportions of nuclear proteins are expelled to the cytoplasm. (d) Proteins with substantial changes in abundance in both compartments, only a minority of which (10 of 77, Figure 6A) show >2-fold changes in both compartments. We propose (see below) that proteins in classes (b) and (c) represent messengers that transmit information about cellular state between the nucleus and other subcellular locations, and note that although they involve smaller proportions of proteins, their influence on cellular function can be important due to strong nonlinearities in cellular function. Proteins in class (d) might represent balancers of overall functional states that may have relevance to many stimulations beyond exposure to estradiol (see below). An important point is that the proteins in classes (b)–(d) are essentially invisible in measurements of total abundance by proteomics or transcriptomics methods. The subcellular spatial razor is excellently suited to detecting them. There is certainly still room for experimental improvement in proteome coverage (quantitation of more proteins in multiple locations), in subcellular fractionation, and in complete protein extraction of fractions. The conservation of mass test in the spatial razor framework provides a very strong filter for identifying reliably detected changes in abundance at different subcellular locations, even if minor proportions of the total protein abundance are involved. We anticipate that this framework can be used to further improve and validate proteomics extraction protocols (see Supporting Information).

Overall, the present results and a number of other recent results on the static and dynamic subcellular spatial distribution of proteins (see below) suggest that extensive dynamic spatial redistribution of proteins is a fundamental characteristic of cellular response that should be considered in system biology analyses of cellular function.

4.2. Protein Subcellular Distribution and Integration of Function

There is increasing evidence that substantial proportions of cellular proteins have multiple subcellular locations and may have different functional roles in different locations. This is implicit in available database information where, for example, 36% of human proteins with current GO CC annotation show multiple locations at the level {nucleus, cytoplasm, plasma membrane, and extracellular region}. There are innumerable studies showing that specific individual proteins show changes in subcellular location and alternative functions in response to cellular environment. For example, over half of the proteins involved in the

glycolysis/gluconeogenesis enzymatic cascade are known to have alternative functions in the nucleus,[16] including in processes connected to hypoxia, proliferation, and cancer.[44,45] Evidence that systematic dynamic changes in the subcellular locations of large numbers of proteins are connected to cellular response/function is beginning to be recorded. For example, over 200 yeast proteins involved in a wide range of cellular functions show subcellular spatial translocation in response to hypoxia.[9] We have shown that a variety of initially surprising proteins show changes in nucleus/cytoplasm distribution when primary human fibroblasts (IMR90 cells) are subjected to cell cycle arrest at the origin activation checkpoint[10] or to oxidative stress (Baqader et al., in preparation). In short, dynamic changes in the subcellular distribution of numerous proteins in response to cellular environment are an increasingly well-established phenomenon. It is noteworthy that in these previous studies 2–5% of monitored proteins were found to show appreciable spatial redistribution in response to various stimulations. The roughly 20% of proteins for which such redistribution was detected in the present experiments is so far a striking outlier, which may reflect that MCF7 cells are cancer cells. There is a clear need for many more global studies of dynamic protein distribution for a variety of cell types and functional contexts.

In the present experiments, the salient question for the over 230 proteins of types (b) and (c) that we identified (Figure 6A) is: do the proportions of these proteins in the “wrong” location relative to their presently defined dominant locations/functions have functional importance? This can ultimately only be answered by further experiments directed at these proteins, but we note that the concept of moonlighting proteins[46] has been actively discussed for over ten years now. Perhaps the most completely studied example at present is the glycolytic enzyme GAPDH, where there has been extensive study of its participation in (a) nuclear transcriptional complexes related to highly controlled S-phase histone transcription,[12,47] (b) association under stress conditions with Siah, an E3-ubiquitinligase, causing the translocation of the complex to the nucleus and subsequently the induction of cellular death/dysfunction,[14,48] and (c) interaction with apurinic/apyrimidinic endonuclease (APE1), leading to the DNA repair functions and to a role in maintaining the integrity of the genome.[49] There is evidence for further functional roles of GAPDH in diverse subcellular locations.[13,14] Other recently elucidated examples of crucial moonlighting proteins are the glycolytic enzymes PKM2 and PFKFB3. Nuclear PKM2 is crucial to the response to hypoxia through participation in transcription complexes with HIFα,[44] regulates β-catenin,[50] and, given its participation in Oct4 transcription complexes,[51] may also have other nuclear functions. Nuclear PFKFB3 appears to play crucial roles in CDK-linked cellular proliferation[52] and in balancing glutamine/glycolysis usage over the cell cycle, including in cancer cells.[53]

Such moonlighting activities are often not predictable by presently defined functional networks, and so far they have mostly been discovered on a case by case basis. The subcellular spatial razor provides a framework for systematic discovery of such proteins, and the present results suggest that many more proteins may have moonlighting roles in the nucleus that are crucial to specific cellular functions. For example, the presence of NQO1 in the nucleus and its redistribution to the cytoplasm with 4-fold reduction in nuclear abundance upon exposure to estradiol, its participation in regulation of the ornithine

decarboxylase complex (ODC), and hence participation in polyamine metabolism,[54] plus the influence of ODC on estrogen receptor (ERα) expression,[55] represent one interesting candidate for moonlighting in the present data. There is a little evidence consistent with nuclear moonlighting roles for NQO1. It is primarily a cytoplasmic protein, but it has been observed associated with mitotic spindles in the nuclei of a variety of human cells where it has been suggested to possibly play roles in protection against electrophic quinones, aid in the generation of oxidized pyridine nucleotides, or shield selected proteins from proteasomal degradation.[56] PARK7 and the 5 enzymes of glycolysis that redistribute to the cytoplasm following estradiol exposure are other moonlighting candidates. In fact, there were a further 60 proteins in the 134-set that Reactome did not place in known functional networks and that might represent moonlighting activities.

The present data also suggests that there may be protein complexes and individual proteins that are involved in more general balancing of cellular function. The demonstration that numerous proteasomal proteins redistribute in response to estradiol and the participation of these proteins in numerous critical functions in both the cytoplasm and nucleus (Table 2) suggests that redistribution of proteasomal subunits may represent general mechanisms for balancing different cellular functions at different subcellular locations. Proteasomal degradation of ERα is an important response to estradiol, and it may be that the complexity of this[57-59] reflects subcellular mobility of proteasome components in addition to many other influences. The redistribution of the CCT protein-folding complex between the nucleus/cytoplasm (Table 2) may be another such example. Nuclear import and/or activity of some proteins, including nuclear hormone receptors,[34,36] involves chaperone-assisted processes, and nucleo-cytoplasmic redistribution of the CCT complex is also observed in the response of primary human fibroblasts to oxidative stress (Baqader et al., in preparation). We also observed redistribution between the nucleus/cytoplasm of numerous chaperones (HSP90B1, HSPA9, HSPB1, HSP90AA1, HSP90AB1, HSPA6, and HSPA8; Supplementary Table S2), and HSP90 chaperones in particular are known to play key roles in nucleocytoplasmic trafficking of nuclear hormone receptors.[34,36] A similar balancing role may be played by some highly abundant proteins such as the human transcriptional positive coactivator PC4 (mammalian orthologue of yeast SUB1), which has established roles in multiple cellular functions involving stabilization of DNA–protein interactions, chromatin organization, transcriptional activation and repression, DNA elongation, reinitiation, and DNA replication and repair.[60-62] This was one of the few proteins to show C $\rightarrow$ N redistribution (without change in total abundance), a phenomenon that we have previously also observed for this protein in the response of primary human fibroblasts to cell cycle arrest at the origin activation checkpoint.[10]

Although not usually discussed as moonlighters, nuclear hormone receptors are inveterate subcellular travelers that have a plethora of nuclear, cytoplasmic, plasma membrane, and mitochondrial activities associated with their mobility. ERs regulate the expression of numerous nuclear genes.[63,64] ERs have plasma membrane interactions that involve numerous kinase-dependent signaling pathways,[36,58,65,66] and there is increasing evidence that these signaling pathways are critical for acquired resistance to therapeutic compounds.[67,68] Cooperative organization of nuclear and mitochondrial ERs and their

coactivators may have crucial influences on regulation of the mitochondrial respiratory chain.[69] Many of these activities seem to be directly associated with subcellular mobility of ER and other proteins. For example, efflux of ERα from the nucleus is associated with repression of cell cycle progression and S-phase proliferation in MCF7 cells.[70,71]

We note that in general nuclear hormone receptors (NHRs) show many of the characteristics that would be expected for proteins with important roles in polling, integrating, and balancing functions occurring at different subcellular locations. They appear to shuttle between different locations and may have many different localization determinants, e.g., different nuclear import/export sequences and pathways[34,35] including ERα.[36] They are often subject to a large variety of posttranslational modifications. In the case of ERα, these include phosphorylation, acetylation, ubiquitination, sumoylation, methylation, and palmitoylation in at least 22 sites.[58] Many of these sites are subject to alternative types of modifications and/or modification by alternative kinases in the case of phosphorylation.[58] It is possible that such post-translational modifications relay information about the functional state between different functions/subcellular locations either directly by carrier NHRs or indirectly via the subcellular localization of the proteins executing the modifications. The lifetime of NHRs may also be consistent with continuous polling of functional state, e.g., in the absence of estrogen ERα is very stable, with a half-life of up to 5 days.[31] This drops to 3–5 h in the presence of estradiol, and the receptors are targeted for degradation through a transcription-coupled pathway requiring new protein synthesis.[31,57,72] In the nucleus NHRs are mobile and characterized by transient interactions with numerous chromatin response elements.[73-75] For ERα, many of the early response chromatin binding sites are only transiently occupied and may be abortive or result in repression,[76] which may reflect the presence of appropriate cofactors in the nucleus. Furthermore, in the nucleus, ERα and ERβ have been shown to interact with 498 other proteins, only 70 of which are common to both.[77] Of these proteins, 357 were detected in the present experiments: with a minimum of 5 SILAC ratio counts, 58 proteins show >2-fold decrease in nuclear abundance, and a further 76 show appreciable nucleo-cytoplasmic redistribution ($|\log_2(S_n/S_c)| > 1$). The present results then suggest that the outcome of the polling by ERs is likely to be dependent on the nuclear/cytoplasm distribution of numerous other proteins as a function of cellular state. It seems likely that other NHRs fulfill similar polling roles, which may include cross-talk between different NHRs.[78]

Attempts have been made to use protein–protein interaction (PPI) networks to analyze cellular response to various nuclear hormone receptors. Almost 20% of the proteins involved were connected to chaperone/nuclear import machinery, and many have multiple subcellular locations,[34] which emphasize further the importance of dynamic subcellular distribution of proteins. The authors concluded that whole cell analyses only allowed limited inferences and that new high-throughput methodologies that monitor different subcellular locations are needed.[34] The proteomics subcellular spatial razor is able to provide the kind of information required.

4.3. Possible Relationships to Breast Cancer

The present results indicate that in MCF7 cells estradiol causes many more substantial changes in subcellular protein distribution than have previously been appreciated. Indeed, the dominant response to estradiol appears to be changes in compartmentalized protein abundances rather than in total protein abundance, including numerous proteins that are present in both the nucleus and mitochondria. This pattern is consistent with other recent proteomics studies. For 76 proteins involved in central metabolic roles in MCF7 cells, time-dependent monitoring of total abundance by proteomics single reaction product methods indicated that none had 2-fold changes in total abundance over the first 24 h of exposure to estradiol.[23] Similarly, study of a tamoxifen resistant MCF7-derivative cell line also showed only a few proteins with >2-fold changes in total abundance compared to the parent MCF7 cells.[55] Finally, although many proteins showed small changes, only moderate differences in total protein abundance between nontumorigenic MCF10A, MCF7, and highly invasive MDA-MB-231 cells were found.[79,80] Recent work has shown that miRNAs may also play a role in regulation of protein expression and in the initiation and progression of breast cancer,[81] but at the level of mRNA, study of the miR-191/425 cluster also found very few proteins with 2-fold changes in total abundance.[82] Taken together with the present results, this suggests that the modified metabolic properties of cancerous MCF7 cells may be mainly based on perturbed spatial distribution of proteins and opens the possibility that transformation and tumorigenicity may also be strongly influenced by perturbed spatial distribution of proteins. Refocusing on the dominant mechanism of cellular response to estradiol may have strong implications for development of therapeutic compounds.

Much recent work on the role of estrogen in breast cancer has focused on the relative importance of ER-dependent activities versus direct genotoxic effects of estrogen metabolites, with both seemingly relevant.[83] Chromatin organization is highly linked to cellular state and to subcellular distribution of proteins, and recent work has shown strong epigenetic changes in the chromatin landscape related to estrogen response and resistance to endocrine therapy.[84] In short, both of the presently most discussed mechanisms for involvement of estrogen in breast cancer could be influenced by major perturbations in subcellular protein spatial organization. Whether highly perturbed spatial distributions are a byproduct or represent a facilitator for transformation/tumorigenicity remains to be investigated. An intriguing observation is that cells may be transformed by perturbations in nucleocytoplasmic shuttling of nuclear hormone receptors and other proteins.[35,85,86]

Supplementary Material

Refer to Web version on PubMed Central for supplementary material.

ACKNOWLEDGMENTS

We would like to thank the Faculty of Agriculture, University of Naples Federico II and the Center for Nephrology, UCL for financial support to G.P., the King Faisal Foundation, Saudi Arabia for supporting A.T.Q., the Cultural Bureau of Saudi Arabia for supporting A.A.M.A., and the Wellcome Trust, U.K. for support to J.G.-Z.

Europe PMC Funders Author Manuscripts

REFERENCES

(1). Colditz GA. Relationship between estrogen levels, use of hormone replacement therapy, and breast cancer. J. Natl. Cancer Inst. 1998; 90:814–823. [PubMed: 9625169]

(2). Henderson BE, Bernstein L. The international variation in breast cancer rates: an epidemiological assessment. Breast cancer Res. Treat. 1991; 18(Suppl1):S11–17. [PubMed: 1873546]

(3). Chen EI, Yates JR III. Cancer proteomics by quantitative shotgun proteomics. Mol. Oncol. 2007; 1:144–159. [PubMed: 18443658]

(4). Laronga C, Drake RR. Proteomic approach to breast cancer. Cancer Control: Journal of the Moffitt Cancer Center. 2007; 14:360–368. [PubMed: 17914336]

(5). Foss EJ, Radulovic D, Shaffer SA, Goodlett DR, Kruglyak L, Bedalov A. Genetic variation shapes protein networks mainly through non-transcriptional mechanisms. PLoS Biol. 2011; 9:e1001144. [PubMed: 21909241]

(6). Shaw RJ, Cantley LC. Decoding key nodes in the metabolism of cancer cells: sugar & spice and all things nice. F1000 Biol. Rep. 2012; 4:2. [PubMed: 22242042]

(7). Dumitrescu RG. DNA methylation and histone modifications in breast cancer. Methods Mol. Biol. 2012; 863:35–45. [PubMed: 22359286]

(8). Liu X, Luo M, Wu K. Epigenetic interplay of histone modifications and DNA methylation mediated by HDA6. Plant Signaling Behav. 2012; 7:633–635.

(9). Henke RM, Dastidar RG, Shah A, Cadinu D, Yao X, Hooda J, Zhang L. Hypoxia elicits broad and systematic changes in protein subcellular localization. Am. J. Physiol., Cell Physiol. 2011; 301:C913–C928. [PubMed: 21753182]

(10). Mulvey CM, Tudzarova S, Crawford M, Williams GH, Stoeber K, Godovac-Zimmermann J. Subcellular proteomics reveals a role for nucleo-cytoplasmic trafficking at the DNA replication origin activation checkpoint. J. Proteome Res. 2013; 12:1436–1453. [PubMed: 23320540]

(11). Chu HY, Hopper AK. Genome-wide investigation of the role of the tRNA nuclear-cytoplasmic trafficking pathway in regulation of the yeast *Saccharomyces cerevisiae* transcriptome and proteome. Mol. Cell. Biol. 2013; 33:4241–4254. [PubMed: 23979602]

(12). He H, Lee MC, Zheng LL, Zheng L, Luo Y. Integration of the metabolic/redox state, histone gene switching, DNA replication and S-phase progression by moonlighting metabolic enzymes. Biosci. Rep. 2012; 33:e00018. [PubMed: 23134369]

(13). Sirover MA. Subcellular dynamics of multifunctional protein regulation: mechanisms of GAPDH intracellular translocation. J. Cell. Biochem. 2012; 113:2193–2200. [PubMed: 22388977]

(14). Tristan C, Shahani N, Sedlak TW, Sawa A. The diverse functions of GAPDH: views from different subcellular compartments. Cell. Signalling. 2011; 23:317–323. [PubMed: 20727968]

(15). Qattan AT, Mulvey C, Crawford M, Natale DA, Godovac-Zimmermann J. Quantitative organelle proteomics of MCF-7 breast cancer cells reveals multiple subcellular locations for proteins in cellular functional processes. J. Proteome Res. 2010; 9:495–508. [PubMed: 19911851]

(16). Qattan AT, Radulovic M, Crawford M, Godovac-Zimmermann J. Spatial distribution of cellular function: the partitioning of proteins between mitochondria and the nucleus in MCF7 breast cancer cells. J. Proteome Res. 2012; 11:6080–6101. [PubMed: 23051583]

(17). Sorokin AV, Kim ER, Ovchinnikov LP. Nucleocytoplasmic transport of proteins. Biokhimiia. 2007; 72:1439–1457.

(18). Thompson ME. BRCA1 16 years later: nuclear import and export processes. FEBS J. 2010; 277:3072–3078. [PubMed: 20608972]

(19). Hamelers I, van Schaik R, Sussenbach J, Steenbergh P. 17beta-Estradiol responsiveness of MCF-7 laboratory strains is dependent on an autocrine signal activating the IGF type I receptor. Cancer Cell Int. 2003; 3:10. [PubMed: 12890289]

(20). Hu ZZ, Kagan BL, Ariazi EA, Rosenthal DS, Zhang LH, Li JV, Huang HZ, Wu C, Jordan VC, Riegel AT, Wellstein A. Proteomic analysis of pathways involved in estrogen-induced growth and apoptosis of breast cancer cells. Plos One. 2011; 6:e20410. [PubMed: 21738574]

(21). Rivenzon-Segal D, Boldin-Adamsky S, Seger D, Seger R, Degani H. Glycolysis and glucose transporter 1 as markers of response to hormonal therapy in breast cancer. Int. J. Cancer. 2003; 107:177–182. [PubMed: 12949791]

(22). Joe I, Ramirez VD. Binding of estrogen and progesterone-BSA conjugates to glyceraldehyde-3-phosphate dehydrogenase (GAPDH) and the effects of the free steroids on GAPDH enzyme activity: physiological implications. Steroids. 2001; 66:529–538. [PubMed: 11182142]

(23). Drabovich AP, Pavlou MP, Dimitromanolakis A, Diamandis EP. Quantitative analysis of energy metabolic pathways in MCF-7 breast cancer cells by selected reaction monitoring assay. Mol. Cell. Proteomics. 2012; 11:422–434. [PubMed: 22535206]

(24). Nilsson S, Makela S, Treuter E, Tujague M, Thomsen J, Andersson G, Enmark E, Pettersson K, Warner M, Gustafsson JA. Mechanisms of estrogen action. Physiol. Rev. 2001; 81:1535–1565. [PubMed: 11581496]

(25). Parl, FF. Estrogens, Estrogen Receptor and Breast Cancer. IOS Press; Amsterdam, Netherlands: 2000. Estrogen Receptor; p. 57-110.

(26). Kumar V, Chambon P. The estrogen receptor binds tightly to its responsive element as a ligand-induced homodimer. Cell. 1988; 55:145–156. [PubMed: 3167974]

(27). Brown M, Sharp PA. Human estrogen receptor forms multiple protein-DNA complexes. J. biol. chem. 1990; 265:11238–11243. [PubMed: 2358459]

(28). Tora L, White J, Brou C, Tasset D, Webster N, Scheer E, Chambon P. The human estrogen receptor has two independent nonacidic transcriptional activation functions. Cell. 1989; 59:477–487. [PubMed: 2805068]

(29). Cicatiello L, Sica V, Bresciani F, Weisz A. Identification of a specific pattern of “immediate-early” gene activation induced by estrogen during mitogenic stimulation of rat uterine cells. Receptor. 1993; 3:17–30. [PubMed: 8348080]

(30). Hyder SM, Nawaz Z, Chiappetta C, Yokoyama K, Stancel GM. The protooncogene c-jun contains an unusual estrogen-inducible enhancer within the coding sequence. J. Biol. Chem. 1995; 270:8506–8513. [PubMed: 7721748]

(31). Nirmala PB, Thampan RV. Ubiquitination of the rat uterine estrogen receptor: dependence on estradiol. Biochem. Biophys. Res. Commun. 1995; 213:24–31. [PubMed: 7639742]

(32). Lonard DM, Nawaz Z, Smith CL, O’Malley BW. The 26S proteasome is required for estrogen receptor-alpha and coactivator turnover and for efficient estrogen receptor-alpha transactivation. Mol. Cell. 2000; 5:939–948. [PubMed: 10911988]

(33). Wijayaratne AL, McDonnell DP. The human estrogen receptor-alpha is a ubiquitinated protein whose stability is affected differentially by agonists, antagonists, and selective estrogen receptor modulators. J. Biol. Chem. 2001; 276:35684–35692. [PubMed: 11473106]

(34). Echeverria PC, Picard D. Molecular chaperones, essential partners of steroid hormone receptors for activity and mobility. Biochim. Biophys. Acta. 2010; 1803:641–649. [PubMed: 20006655]

(35). Mavinakere MS, Powers JM, Subramanian KS, Roggero VR, Allison LA. Multiple novel signals mediate thyroid hormone receptor nuclear import and export. J. Biol. Chem. 2012; 287:31280–31297. [PubMed: 22815488]

(36). Renoir JM. Estradiol receptors in breast cancer cells: associated co-factors as targets for new therapeutic approaches. Steroids. 2012; 77:1249–1261. [PubMed: 22917634]

(37). Shevchenko A, Tomas H, Havlis J, Olsen JV, Mann M. In-gel digestion for mass spectrometric characterization of proteins and proteomes. Nat. Protoc. 2006; 1:2856–2860. [PubMed: 17406544]

(38). Cox J, Mann M. MaxQuant enables high peptide identification rates, individualized p.p.b.-range mass accuracies and proteome-wide protein quantification. Nat. Biotechnol. 2008; 26:1367–1372. [PubMed: 19029910]

(39). Cox J, Matic I, Hilger M, Nagaraj N, Selbach M, Olsen JV, Mann M. A practical guide to the MaxQuant computational platform for SILAC-based quantitative proteomics. Nat. Protoc. 2009; 4:698–705. [PubMed: 19373234]

(40). Croft D, O’Kelly G, Wu G, Haw R, Gillespie M, Matthews L, Caudy M, Garapati P, Gopinath G, Jassal B, Jupe S, Kalatskaya I, Mahajan S, May B, Ndegwa N, Schmidt E, Shamovsky V, Yung

C, Birney E, Hermjakob H, D'Eustachio P, Stein L. Reactome: a database of reactions, pathways and biological processes. Nucleic Acids Res. 2011; 39:D691–697. [PubMed: 21067998]

(41). Milacic M, Haw R, Rothfels K, Wu G, Croft D, Hermjakob H, Eustachio P, Stein L. Annotating cancer variants and anti-cancer therapeutics in reactome. Cancers. 2012; 4:1180–1211. [PubMed: 24213504]

(42). Dopie J, Skarp K-P, Kaisa Rajakylä E, Tanhuanpää K, Vartiainen MK. Active maintenance of nuclear actin by importin 9 supports transcription. Proc. Natl. Acad. Sci. U.S.A. 2012; 109:E544–E552. [PubMed: 22323606]

(43). Dzijak R, Yildirim S, Kahle M, Novak P, Hnilicova J, Venit T, Hozak P. Specific nuclear localizing sequence directs two myosin isoforms to the cell nucleus in calmodulin-sensitive manner. PLoS One. 2012; 7:e30529. [PubMed: 22295092]

(44). Luo W, Semenza GL. Pyruvate kinase M2 regulates glucose metabolism by functioning as a coactivator for hypoxia-inducible factor 1 in cancer cells. Oncotarget. 2011; 2:551–556. [PubMed: 21709315]

(45). Heiden MG, Locasale JW, Swanson KD, Sharfi H, Heffron GJ, Amador-Noguez D, Christofk HR, Wagner G, Rabinowitz JD, Asara JM, Cantley LC. Evidence for an alternative glycolytic pathway in rapidly proliferating cells. Science. 2010; 329:1492–1499. [PubMed: 20847263]

(46). Jeffery CJ. Moonlighting proteins: an update. Mol. BioSyst. 2009; 5:345–350. [PubMed: 19396370]

(47). Zheng L, Roeder RG, Luo Y. S phase activation of the histone H2B promoter by OCA-S, a coactivator complex that contains GAPDH as a key component. Cell. 2003; 114:255–266. [PubMed: 12887926]

(48). Hara MR, Snyder SH. Nitric oxide-GAPDH-Siah: a novel cell death cascade. Cell. Mol. Neurobiol. 2006; 26:527–538. [PubMed: 16633896]

(49). Azam S, Jouvet N, Jilani A, Vongsamphanh R, Yang X, Yang S, Ramotar D. Human glyceraldehyde-3-phosphate dehydrogenase plays a direct role in reactivating oxidized forms of the DNA repair enzyme APE1. J. Biol. Chem. 2008; 283:30632–30641. [PubMed: 18776186]

(50). Yang W, Xia Y, Ji H, Zheng Y, Liang J, Huang W, Gao X, Aldape K, Lu Z. Nuclear PKM2 regulates beta-catenin transactivation upon EGFR activation. Nature. 2011; 480:118–122. [PubMed: 22056988]

(51). Lee J, Kim HK, Han YM, Kim J. Pyruvate kinase isozyme type M2 (PKM2) interacts and cooperates with Oct-4 in regulating transcription. Int. J. Biochem. Cell Biol. 2008; 40:1043–1054. [PubMed: 18191611]

(52). Yalcin A, Clem BF, Simmons A, Lane A, Nelson K, Clem AL, Brock E, Siow D, Wattenberg B, Telang S, Chesney J. Nuclear targeting of 6-phosphofructo-2-kinase (PFKFB3) increases proliferation via cyclin-dependent kinases. J. Biol. Chem. 2009; 284:24223–24232. [PubMed: 19473963]

(53). Colombo SL, Palacios-Callender M, Frakich N, Carcamo S, Kovacs I, Tudzarova S, Moncada S. Molecular basis for the differential use of glucose and glutamine in cell proliferation as revealed by synchronized HeLa cells. Proc. Natl. Acad. Sci. U.S.A. 2011; 108:21069–21074. [PubMed: 22106309]

(54). Asher G, Bercovich Z, Tsvetkov P, Shaul Y, Kahana C. 20S proteasomal degradation of ornithine decarboxylase is regulated by NQO1. Mol. cell. 2005; 17:645–655. [PubMed: 15749015]

(55). Zhu Q, Jin L, Casero RA, Davidson NE, Huang Y. Role of ornithine decarboxylase in regulation of estrogen receptor alpha expression and growth in human breast cancer cells. Breast Cancer Res. Treat. 2012; 136:57–66. [PubMed: 22976807]

(56). Siegel D, Kepa JK, Ross D. NAD(P)H:quinone oxidoreductase 1 (NQO1) localizes to the mitotic spindle in human cells. PLoS One. 2012; 7:e44861. [PubMed: 22984577]

(57). Alarid ET. Lives and times of nuclear receptors. Mol. Endocrinol. 2006; 20:1972–1981. [PubMed: 16423879]

(58). Le Romancer M, Poulard C, Cohen P, Sentis S, Renoir JM, Corbo L. Cracking the estrogen receptor's posttranslational code in breast tumors. Endocrine Rev. 2011; 32:597–622. [PubMed: 21680538]

(59). Nonclercq D, Journe F, Laios I, Chaboteaux C, Toillon RA, Leclercq G, Laurent G. Effect of nuclear export inhibition on estrogen receptor regulation in breast cancer cells. J. Mol. Endocrinol. 2007; 39:105–118. [PubMed: 17693610]

(60). Conesa C, Acker J. Sub1/PC4 a chromatin associated protein with multiple functions in transcription. RNA Biol. 2010; 7:287–290. [PubMed: 20305379]

(61). Das C, Hizume K, Batta K, Kumar BR, Gadad SS, Ganguly S, Lorain S, Verreault A, Sadhale PP, Takeyasu K, Kundu TK. Transcriptional coactivator PC4, a chromatin-associated protein, induces chromatin condensation. Mol. Cell. Biol. 2006; 26:8303–8315. [PubMed: 16982701]

(62). Malik S, Guermah M, Roeder RG. A dynamic model for PC4 coactivator function in RNA polymerase II transcription. Proc. Natl. Acad. Sci. U.S.A. 1998; 95:2192–2197. [PubMed: 9482861]

(63). Frasor J, Danes JM, Komm B, Chang KC, Lyttle CR, Katzenellenbogen BS. Profiling of estrogen up- and down-regulated gene expression in human breast cancer cells: insights into gene networks and pathways underlying estrogenic control of proliferation and cell phenotype. Endocrinology. 2003; 144:4562–4574. [PubMed: 12959972]

(64). Marino M, Galluzzo P, Ascenzi P. Estrogen signaling multiple pathways to impact gene transcription. Curr. Genomics. 2006; 7:497–508. [PubMed: 18369406]

(65). Heldring N, Pike A, Andersson S, Matthews J, Cheng G, Hartman J, Tujague M, Strom A, Treuter E, Warner M, Gustafsson JA. Estrogen receptors: how do they signal and what are their targets. Physiol. Rev. 2007; 87:905–931. [PubMed: 17615392]

(66). Madak-Erdogan Z, Kieser KJ, Kim SH, Komm B, Katzenellenbogen JA, Katzenellenbogen BS. Nuclear and extranuclear pathway inputs in the regulation of global gene expression by estrogen receptors. Mol. Endocrinol. 2008; 22:2116–2127. [PubMed: 18617595]

(67). Iorns E, Turner NC, Elliott R, Syed N, Garrone O, Gasco M, Tutt AN, Crook T, Lord CJ, Ashworth A. Identification of CDK10 as an important determinant of resistance to endocrine therapy for breast cancer. Cancer Cell. 2008; 13:91–104. [PubMed: 18242510]

(68). Yeh WL, Shioda K, Coser KR, Rivizzigno D, McSweeney KR, Shioda T. Fulvestrant-induced cell death and proteasomal degradation of estrogen receptor alpha protein in MCF-7 cells require the CSK c-Src tyrosine kinase. PLoS One. 2013; 8:e60889. [PubMed: 23593342]

(69). Chen JQ, Cammarata PR, Baines CP, Yager JD. Regulation of mitochondrial respiratory chain biogenesis by estrogens/estrogen receptors and physiological, pathological and pharmacological implications. Biochim. Biophys. Acta. 2009; 1793:1540–1570. [PubMed: 19559056]

(70). Castoria G, Migliaccio A, Auricchio F. Signaling-dependent nuclear export of estradiol receptor controls cell cycle progression in breast cancer cells. Mol. Cell. Endocrinol. 2009; 308:26–31. [PubMed: 19549589]

(71). Lombardi M, Castoria G, Migliaccio A, Barone MV, Di Stasio R, Ciociola A, Bottero D, Yamaguchi H, Appella E, Auricchio F. Hormone-dependent nuclear export of estradiol receptor and DNA synthesis in breast cancer cells. J. Cell Biol. 2008; 182:327–340. [PubMed: 18644889]

(72). Alarid ET, Bakopoulos N, Solodin N. Proteasome-mediated proteolysis of estrogen receptor: a novel component in autologous down-regulation. Mol. Endocrinol. 1999; 13:1522–1534. [PubMed: 10478843]

(73). Elbi C, Walker DA, Romero G, Sullivan WP, Toft DO, Hager GL, DeFranco DB. Molecular chaperones function as steroid receptor nuclear mobility factors. Proc. Natl. Acad. Sci. U.S.A. 2004; 101:2876–2881. [PubMed: 14978266]

(74). McNally JG, Muller WG, Walker D, Wolford R, Hager GL. The glucocorticoid receptor: rapid exchange with regulatory sites in living cells. Science. 2000; 287:1262–1265. [PubMed: 10678832]

(75). Reid G, Hubner MR, Metivier R, Brand H, Denger S, Manu D, Beaudouin J, Ellenberg J, Gannon F. Cyclic, proteasome-mediated turnover of unliganded and liganded ERalpha on responsive promoters is an integral feature of estrogen signaling. Mol. Cell. 2003; 11:695–707. [PubMed: 12667452]

(76). Stossi F, Madak-Erdogan Z, Katzenellenbogen BS. Estrogen receptor alpha represses transcription of early target genes via p300 and CtBP1. Mol. Cell. Biol. 2009; 29:1749–1759. [PubMed: 19188451]

(77). Nassa G, Tarallo R, Guzzi PH, Ferraro L, Cirillo F, Ravo M, Nola E, Baumann M, Nyman TA, Cannataro M, Ambrosino C, Weisz A. Comparative analysis of nuclear estrogen receptor alpha and beta interactomes in breast cancer cells. Mol. BioSyst. 2011; 7:667–676. [PubMed: 21173974]

(78). Bolt MJ, Stossi F, Newberg JY, Orjalo A, Johansson HE, Mancini MA. Coactivators enable glucocorticoid receptor recruitment to fine-tune estrogen receptor transcriptional responses. Nucleic Acids Res. 2013; 41:4036–4048. [PubMed: 23444138]

(79). Bateman NW, Sun M, Hood BL, Flint MS, Conrads TP. Defining central themes in breast cancer biology by differential proteomics: conserved regulation of cell spreading and focal adhesion kinase. J. Proteome Res. 2010; 9:5311–5324. [PubMed: 20681588]

(80). Pavlou MP, Dimitromanolakis A, Diamandis EP. Coupling proteomics and transcriptomics in the quest of subtype-specific proteins in breast cancer. Proteomics. 2013; 13:1083–1095. [PubMed: 23386393]

(81). Klinge CM. miRNAs and estrogen action. Trends Endocrinol. Metab. 2012; 23:223–233. [PubMed: 22503553]

(82). Di Leva G, Piovan C, Gasparini P, Ngankeu A, Taccioli C, Briskin D, Cheung DG, Bolon B, Anderlucci L, Alder H, Nuovo G, Li M, Iorio MV, Galasso M, Santhanam R, Marcucci G, Perrotti D, Powell KA, Bratasz A, Garofalo M, Nephew KP, Croce CM. Estrogen mediated-activation of miR-191/425 cluster modulates tumorigenicity of breast cancer cells depending on estrogen receptor status. PLoS Genetics. 2013; 9:e1003311. [PubMed: 23505378]

(83). Yue W, Yager JD, Wang JP, Jupe ER, Santen RJ. Estrogen receptor-dependent and independent mechanisms of breast cancer carcinogenesis. Steroids. 2013; 78:161–170. [PubMed: 23178278]

(84). Magnani L, Stoeck A, Zhang X, Lanczky A, Mirabella AC, Wang TL, Gyorffy B, Lupien M. Genome-wide reprogramming of the chromatin landscape underlies endocrine therapy resistance in breast cancer. Proc. Natl. Acad. Sci. U.S.A. 2013; 110:E1490–1499. [PubMed: 23576735]

(85). Bonamy GM, Allison LA. Oncogenic conversion of the thyroid hormone receptor by altered nuclear transport. Nucl. Recept. Signaling. 2006; 4:e008.

(86). Bonamy GM, Guiochon-Mantel A, Allison LA. Cancer promoted by the oncoprotein v-ErbA may be due to subcellular mislocalization of nuclear receptors. Mol. Endocrinol. 2005; 19:1213–1230. [PubMed: 15650025]

Europe PMC Funders Author Manuscripts

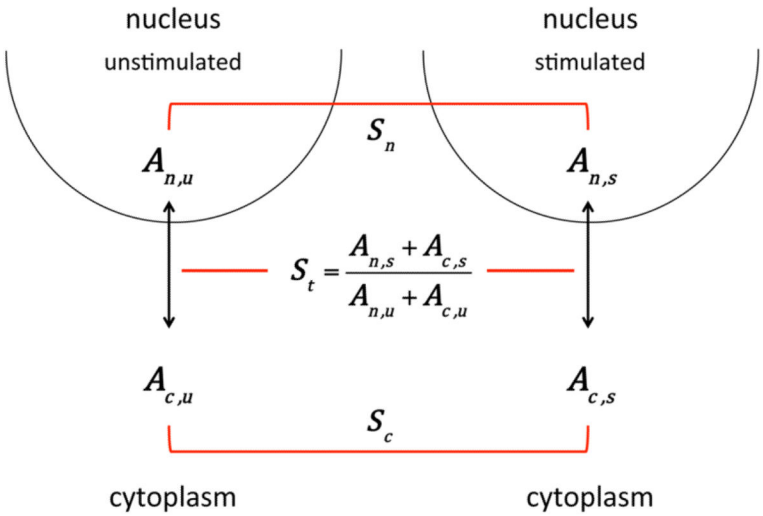

Figure 1.

Subcellular spatial razor model. A protein (A) has different abundances in unstimulated (u) or stimulated (s) cells and in the nucleus (n) or in the cytoplasm (c). The ratio of the abundance of the protein between unstimulated/stimulated cells is measured by SILAC isotope ratios for the nucleus (S_n), the cytoplasm (S_c), and for a total cell lysate (S_t).

Europe PMC Funders Author Manuscripts

Europe PMC Funders Author Manuscripts

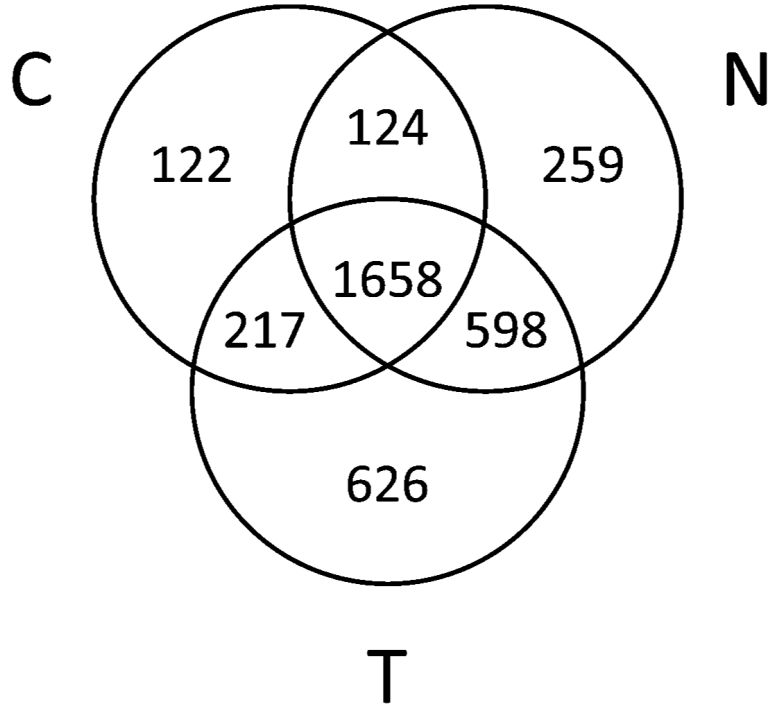

Figure 2.
Venn diagram of the distribution over sample types for proteins quantified with ≥3 SILAC ratio counts in each sample.

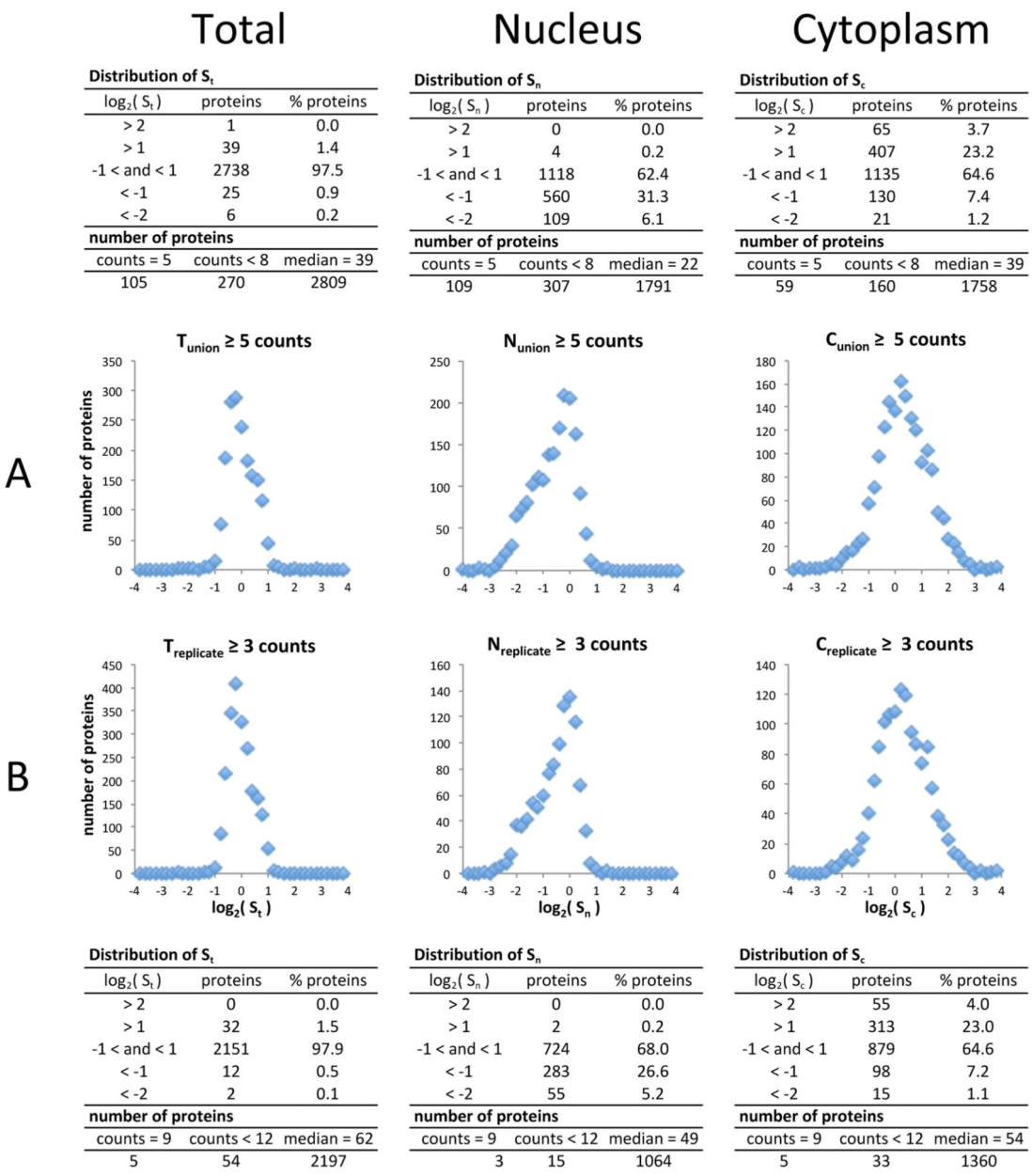

Distribution of S_t

$\log_2(S_t)$	proteins	% proteins
> 2	1	0.0
> 1	39	1.4
-1 < and < 1	2738	97.5
< -1	25	0.9
< -2	6	0.2

number of proteins

counts = 5	counts < 8	median = 39
105	270	2809

Distribution of S_n

$\log_2(S_n)$	proteins	% proteins
> 2	0	0.0
> 1	4	0.2
-1 < and < 1	1118	62.4
< -1	560	31.3
< -2	109	6.1

number of proteins

counts = 5	counts < 8	median = 22
109	307	1791

Distribution of S_c

$\log_2(S_c)$	proteins	% proteins
> 2	65	3.7
> 1	407	23.2
-1 < and < 1	1135	64.6
< -1	130	7.4
< -2	21	1.2

number of proteins

counts = 5	counts < 8	median = 39
59	160	1758

Distribution of S_t

$\log_2(S_t)$	proteins	% proteins
> 2	0	0.0
> 1	32	1.5
-1 < and < 1	2151	97.9
< -1	12	0.5
< -2	2	0.1

number of proteins

counts = 9	counts < 12	median = 62
5	54	2197

Distribution of S_n

$\log_2(S_n)$	proteins	% proteins
> 2	0	0.0
> 1	2	0.2
-1 < and < 1	724	68.0
< -1	283	26.6
< -2	55	5.2

number of proteins

counts = 9	counts < 12	median = 49
3	15	1064

Distribution of S_c

$\log_2(S_c)$	proteins	% proteins
> 2	55	4.0
> 1	313	23.0
-1 < and < 1	879	64.6
< -1	98	7.2
< -2	15	1.1

number of proteins

counts = 9	counts < 12	median = 54
5	33	1360

Figure 3.

Distribution of SILAC ratios for proteins from the total lysate (S_t), nuclear (S_n), and cytoplasmic (S_c) samples. (A) All proteins with ≥5 ratio counts for the union of the three replicates for each sample type. (B) All proteins with ≥3 ratio counts for all replicates of each sample type. The inset tables show the number and percentage of proteins that show >4-fold or >2-fold changes in total abundance (S_t), nuclear compartment abundance (S_n), and cytoplasmic compartment abundance (S_c). The tables also show for each distribution the total number of proteins included, the median number of SILAC ratio counts, and the number of proteins with smaller numbers of SILAC ratio counts.

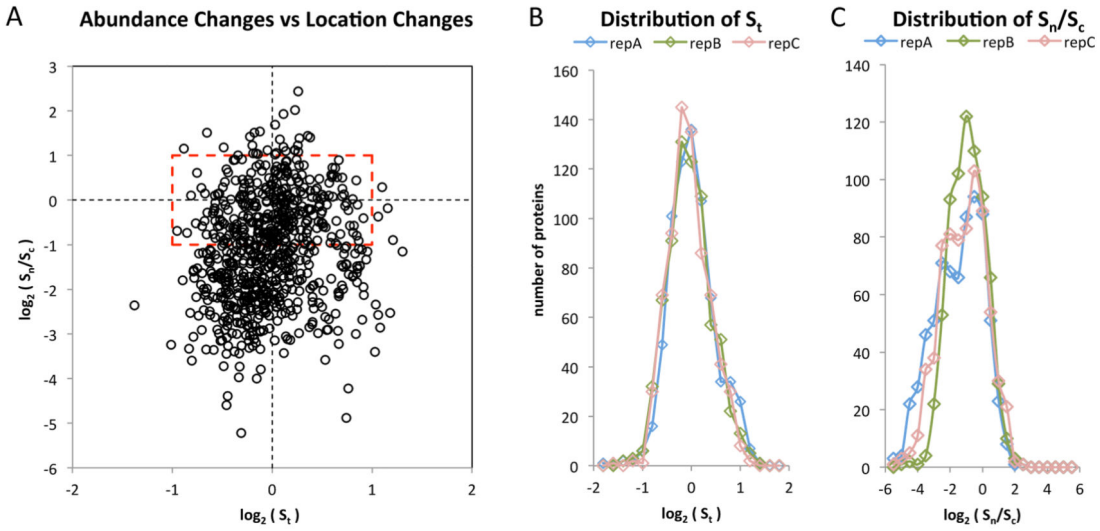

Figure 4.

Evaluation of the correlation between changes in total abundance and redistribution of abundance between the nucleus and cytoplasm. (A) Plot of the redistribution parameter (S_n/S_c) vs the changes in total abundance (S_t) for the union over the replicates. The red, dashed bounding box corresponds to 2-fold changes. (B) Distribution of S_t for the three replicates. (C) Distribution of (S_n/S_c) for the three replicates.

Europe PMC Funders Author Manuscripts

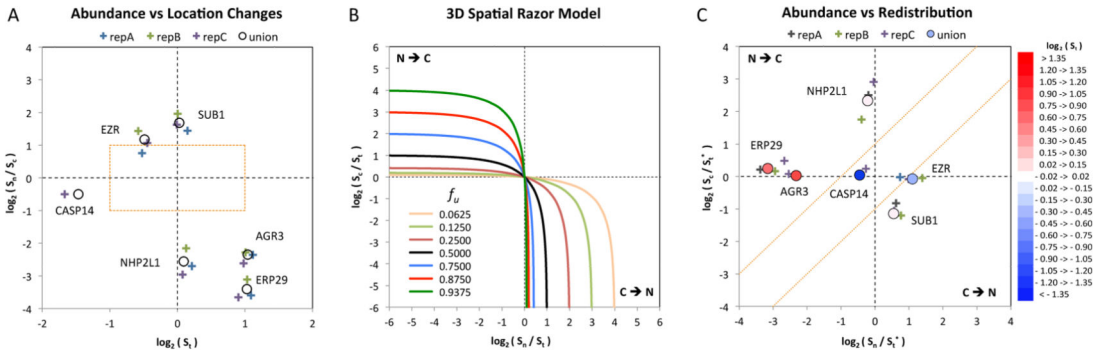

Figure 5.

Two- and three-dimensional data representations for the subcellular spatial razor. (A) Two-dimensional plot of changes in redistribution between the nucleus and cytoplasm (S_n/S_c) versus total abundance (S_t) for six proteins from Figure 4 showing the experimental scatter. The union is the average over the replicates weighted by the MS intensity recorded for the protein in each replicate. The orange bounding box shows 2-fold changes. (B) For the orthogonal 3D space $\{S_n/S_t, S_c/S_t, S_t\}$, the theoretical distribution plane $\{S_n/S_t, S_c/S_t\}$ for different values of f_u (the fraction of protein in the nucleus in the unstimulated cells) as the fraction of the protein in the nucleus in the stimulated cells (f_s) varies over $0 < f_s < 1$. Conservation of mass restricts the cellular response to two quadrants corresponding to N → C or C → N redistribution of the protein upon stimulation (see Supporting Information). (C) The six proteins of panel A plotted in the 3D space $\{S_n/S_t, S_c/S_t, S_t\}$. The axis perpendicular to the page is color coded for changes in total abundance (S_t). The orange bounding lines show 2-fold changes in (S_n/S_c).

Europe PMC Funders Author Manuscripts

Number (%) of proteins with > 2-fold change in compartmental abundance

CT and NT data sets

$\lvert\log_2(S_{c,n}/S_t)\rvert$	total (CT ,NT)	$\log_2(S)$	S_c		S_n		S_n/S_c		S_t (C & N)	
			N	%	N	%	N	%	N	%
< 0.5	56, 169	> 1	1	1.8	1	0.6			2	0.8
< 0.4	45, 145	> 1	0	0	1	0.7			1	0.5
< 0.3	36, 104	> 1	0	0	1	1			1	0.7
< 0.5	56, 169	< -1	3	5.3	2	1.2			0	0.0
< 0.4	45, 145	< -1	2	4.4	2	1.4			0	0.0
< 0.3	36, 104	< -1	1	2.8	0	0			0	0.0

CNT data set

$\lvert\log_2(S_t^*/S_t)\rvert$	total	$\log_2(S)$	S_c		S_n		S_n/S_c		S_t	
			N	%	N	%	N	%	N	%
< 0.5	601	> 1	89	14.8	0	0	11	1.8	2	0.3
< 0.4	493	> 1	70	14.2	0	0	9	1.8	2	0.4
< 0.3	359	> 1	52	14.5	0	0	4	1.1	2	0.5
< 0.5	601	< -1	8	1.3	179	29.7	295	49.1	3	0.5
< 0.4	493	< -1	6	1.2	143	29.0	237	48.1	2	0.4
< 0.3	359	< -1	5	1.4	109	30.3	180	50.1	2	0.5

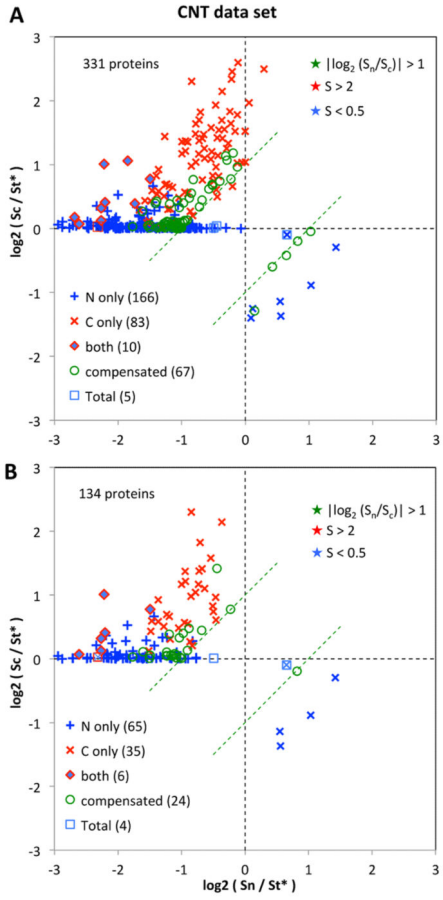

Figure 6.

Table: (top) number of proteins detected in a single subcellular compartment with >2-fold changes in abundance; (bottom) number of proteins detected in both compartments with >2-fold changes in abundance (S_n, S_c, or S_t) or in S_n/S_c. The number of proteins included varies with the selection range around S_n/S_t, S_c/S_t, or $S_t^*/S_t = 1$ (see text). (A) Three-dimensional plot for 331 proteins with $|\log_2(S/S_t)| < 0.5$. (B) Three-dimensional plot for 134 proteins with $|\log_2(S/S_t)| \leq 0.5$ that were quantified with ≥10 SILAC ratio counts in at least two replicates. The legend (lower left) shows the symbol coding for >2-fold changes only in S_n, only in S_c,

in both S_n and S_c, for S_n/S_c only, and for S_t. Increases/decreases are color coded (upper right legend).

Europe PMC Funders Author Manuscripts

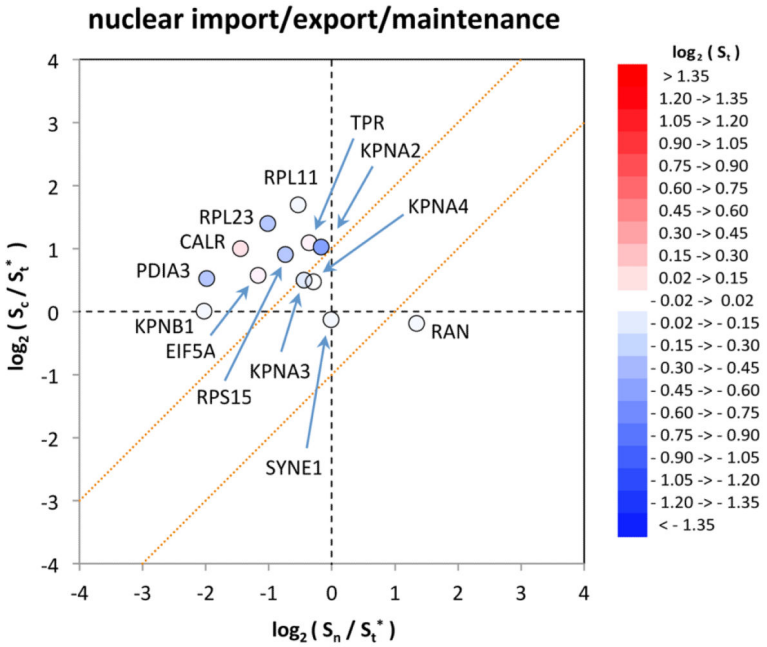

Figure 7.

Three-dimensional spatial razor plot for proteins with GO annotations corresponding to nuclear import/export/localization/maintenance.

Europe PMC Funders Author Manuscripts

Europe PMC Funders Author Manuscripts

Table 1

Distribution of GO CC Annotation for the 134 Protein Set

subcellular location	nucleus	plasma membrane	extracellular region	cytoplasm	cytosol	mitochondrion	endoplasmic reticulum	Golgi apparatus	melanosome	peroxisome	endosome	lysosome
nucleus	66	15	4	58	35	10	2	2	5	1	0	0
plasma membrane		27	4	25	15	2	2	3	4	0	2	2
extracellular region			14	12	7	2	6	1	3	0	0	1
cytoplasm				120	75	19	9	6	9	2	4	5
cytosol					75	8	2	4	6	0	4	2
mitochondrion						19	1	1	3	1	0	0
endoplasmic reticulum							9	1	2	0	0	1
Golgi apparatus								6	0	0	2	1
melanosome									9	0	0	0
peroxisome										2	0	0
endosome											4	1
lysosome												5
GO CC ID	GO:0005634	GO:0005886	GO:0005576	GO:0005737	GO:0005829	GO:0005739	GO:0005783	GO:0005794	GO:0042470	GO:0005777	GO:0005768	GO:0005764

Europe PMC Funders Author Manuscripts

Table 2

Analysis of Functional Groups with Reactome

Reactome Name	number of proteins	Reactome identifier	proteins in identifier	p-value	distribution (Fig. 6)	gene names
MAJOR CATEGORIES						
Metabolism of mRNA	17	REACT_20605	224	2.0E-10		
Metabolism of proteins	22	REACT_17015	574	1.2E-07		
Gene Expression	27	REACT_71	1031	7.0E-06		
Cell Cycle	16	REACT_115566	478	5.0E-05		
CYTOPLASM						
small molecule metabolism						
Glycolysis	5	REACT_1383	27	9.6E-06		ALDOA,ENO1,GAPDH,PGK1,ALDOC
Regulation of ornithine decarboxylase (ODC)	8	REACT_13565	50	5.6E-08		PSMA2,PSMA3,NQO1,PSMA1,PSMB5, PSME1,PSMB6,PSMB7
Vitamins B6 activation to pyridoxal phosphate	2	REACT_25012	3	3.6E-04		PDXK.PNPO
Synthesis and interconversion of nucleotide di- and triphosphates	3	REACT_21330	18	9.3E-04		TXN,TXNRD1,GSR
protein translation						
Translation	11	REACT_1014	151	5.3E-06		EIF2S3L,RPS20,EEF2,EIF2S3,RPL12,RPS7, RPS3,RPS3A,RPS16,EIF4H,EIF2S1
3′ -UTR-mediated translational regulation	10	REACT_1762	109	2.6E-06		EIF2S3L,RPS20,EIF2S3,RPL12,RPS7,RPS3, RPS3A,RPS16,EIF4H,EIF2S1
protein folding						
Cooperation of Prefoldin and TriC/CCT in actin and tubulin folding	8	REACT_17029	27	2.8E-10		CCT2,TUBB4B,CCT6A,CCT3,CCT4,CCT5, TCP1,CCT7
Association of CCT/TriC with other substrates during biosynthesis	7	REACT_16984	48	4.0E-08		CCT2,CCT6A,CCT3,CCT4,CCT5,TCP1, CCT7
mRNA metabolism						

Europe PMC Funders Author Manuscripts

Reactome Name	number of proteins	Reactome identifier	proteins in identifier	p-value	distribution (Fig. 6)	gene names
Regulation of mRNA Stability by Proteins that Bind AU-rich Elements	10	REACT_24994	86	2.6E-08		PSMA2,PSMA3,PSMA1,PSMB5,ANP32A, HSPB1,PSME1,HSPA8,PSMB7,PSMB6
Destabilization of mRNA by AUF1 (hnRNP DO)	9	REACT_25325	54	5.3E-09		PSMA2,PSMA3,PSMA1,PSMB5,HSPB1, PSME1,HSPA8,PSMB7,PSMB6
Nonsense-Mediated Decay	7	REACT_75886	110	1.9E-04		RPS20,RPS3A,RPS16,RPL12,RPS7,RPS3, RBM8A
protein degradation						
Proteasomal clevage of exogenous antigen	7	REACT_111172	44	4.2E-07		PSME1,PSMA2,PSMA3,PSMA1,PSMB5, PSMB7,PSMB6
NUCLEUS						
cell cycle						
Mitotic M-M/G1 phases	10	REACT_21300	266	6.3E-04		TUBB4B,PSMA2,PSMA3,PSMA1,CSNK2B, PSMB5,PSME1,RCC2,PSMB7,PSMB6
Mitotic G1-G1/S phases	8	REACT_21267	133	9.8E-05		PSMA2,PSMA3,PSMA1,PSMB5,PSME1, PSMB6,RBBP4,PSMB7
Nucleosome assembly	S	REACT_22344	45	1.2E-04		NPM1,HIST1H4A,HIST1H2BL,RBBP4, H2BFS
mRNA splicing						
Cleavage at the 3′-Splice Site and Exon Ligation	4	REACT_1331	108	3.1E-02		SF3B3,PCBP2,PCBP1,RBM8A
PLASMA MEMBRANE						
receptors and intercellular interactions						
Signaling by Wnt	9	REACT_11045	91	5.7E-07		PSMA2,PSMA3,PSMA1,PSMB5,PSME1, VPS26A,SNX3,PSMB7,PSMB6
Regulation of actin dynamics for phagocytic cup formation	8	REACT_160086	214	2.3E-03		ACTR3,ARPC5,ARPC3,ACTR2,HSP90AB1,ARPC2,HSP90AA1,ARPC4
Role of myosins in phagosome formation	6	REACT_160090	195	2.0E-02		ACTR3,ARPC5,ARPC2,ARPC3,ACTR2, ARPC4

J Proteome Res. Author manuscript; available in PMC 2014 December 10.

Europe PMC Funders Author Manuscripts

Reactome Name	number of proteins	Reactome identifier	proteins in identifier	p-value	distribution (Fig. 6)	gene names
L1CAM interactions	4	REACT_22205	107	3.0E-02		TUBB4B,HSPA8,CSNK2B,ITGA2